stabilizing CP110 at the distal end of mother centrioles and by remodeling centriolar MTs via its MT-depolymerizing activity (Kobayashi et al., 2011). Therefore, whether the other kinesin-13s play a role in the control of primary cilia disassembly during the proliferative phase remains an open question. In this study, overexpression of each kinesin-13 protein in serum-starved hTERT-RPE1 cells indicated that all members did not equally reduce ciliated cells in the quiescent G0 phase and that KIF2A was able to mediate primary cilia disassembly through its MT-depolymerizing activity with a similar potency to KIF24 (Figures 1A and 1B). Loss of *KIF2A* by TALEN-mediated knockout in hTERT-RPE1 cells caused impairment of primary cilia disassembly following growth stimulation and inappropriate ciliogenesis in the proliferative phase (Figures S2 and S3); thereby, the MT-depolymerizing activity of KIF2A is essential for primary cilia disassembly coupled with cell proliferation and blocking inappropriate ciliogenesis during the cycling phase. However, depletion of *KIF2A* did not completely impair primary cilia disassembly and suppression (Figures S2F, S2G, S3F, and S3G). The mother centriole localization of KIF24, which has the strongest potency to suppress ciliogenesis among kinesin-13 family members (Figures 1A and 1B), is not changed in *KIF2A*-deficient cells (Figure S3I). KIF2A potentially binds to CP110 in vitro as well as KIF24 does (Figure S1D). These data imply that KIF24 redundantly acts in the contexts of KIF2A-mediated cilia disassembly and suppression. Further analyses of all kinesin-13 family members will be required to elucidate how primary cilia disassembly is orchestrated.

How does KIF2A disassemble primary cilia via the MT depolymerizaton? Here, we demonstrate that KIF2A localizes to the subdistal appendages of the mother centrioles during the interphase. However, the subdistal appendages topologically seem unlikely to be the relevant site of microtubule depolymerization for primary cilia disassembly, because they are not the free ends of axonemal microtubules. Recently, it was reported that the subdistal appendages are required for the stabilization of centrosomal (cytoplasmic) MTs during the quiescent phase (Tateishi et al., 2013). One possible mechanism for primary cilia disassembly is that KIF2A at the subdistal appendages might depolymerize centrosomal (cytoplasmic) MTs to arrest transport of materials such as tubulin into cilium (Bhogaraju et al., 2013). Alternatively, it was proposed that cytosolic tubulin concentration modulates cilia length and number (Sharma et al., 2011). Depletion of *KIF2A* did not increase the total amount of tubulin (Figure S2D) but promoted to polymerize cytoplasmic microtubules (Figures S4B–S4D), suggesting that KIF2A controls the cytoplasmic tubulin concentration to regulate primary cilia disassembly. Although further studies are required to clarify how the MT-depolymerizing activity of KIF2A is transmitted to primary cilia disassembly, this study demonstrates that the MT-depolymerizing activity of KIF2A at the mother centriole is a driving force of primary cilia disassembly during the proliferative phase.

Our results indicate that KIF2A is quantitatively controlled by APC/C ubiquitin ligase during the cell cycle. KIF2A levels were relatively low in the quiescent G0 phase but increased during the proliferative phase (Figure S1A). APC/C activity is tightly regulated during the cell cycle through the binding of CDC20 or another coactivator CDH1 (Peters, 2006). CDC20 binds to APC/C in a CDK1/cyclin B-dependent manner to initiate the metaphase-anaphase transition through ubiquitin/proteasome-mediated degradation of securin and cyclin B. By the end of mitosis, APC/C^{CDC20} is no longer active. From late M to G1 and G0 phases, CDH1 preferentially interacts with APC/C to activate the APC/C^{CDH1} ubiquitin ligase activity. Previous studies indicated that APC/C^{CDH1} activity is indispensable for apical docking of the basal body via tuning of the level of its substrate DVL in the context of ciliogenesis during the G0 phase (Ganner et al., 2009; Miyamoto et al., 2011). To the contrary, a recent study demonstrated that CDC20 during the G0 phase localizes to centrosomes to regulate the proper ciliary length and that it is released from centrosomes during the proliferative phase (Wang et al., 2014). We found that KIF2A is ubiquitinated by APC/C during the quiescent G0 phase and its ubiquitination is inhibited to increase the total amount of KIF2A in the proliferative phase. Interestingly, KIF24 expression is also low in the G0/G1 phase (Kobayashi et al., 2011) and this study demonstrates that it binds to an APC/C subunit (Figure S1C), implying that APC/C in the quiescent G0 phase ubiquitinates both KIF2A and KIF24 to robustly suppress premature initiation of cilia disassembly. Thus, PLK1 and APC/C-mediated dual regulation connect the MT-depolymerizing activity of KIF2A to a physiological primary cilia disassembly during the proliferative phase.

Previously, we showed that BUBR1 in the G0 phase mediates ubiquitin-mediated proteasome degradation of CDC20 to regulate the optimal level of DVL proteins for apical docking of the basal body in ciliogenesis and, consequently, high levels of DVLs in the PCS (MVA) syndrome patient cells block primary cilia formation (Miyamoto et al., 2011). We also showed that, in the interphase, BUBR1 localizes to centrosomes to inhibit PLK1 activity (Izumi et al., 2009) and that the PCS (MVA) syndrome

Figure 3. PLK1-Mediated KIF2A Phosphorylation Occurs at the Mother Centriole following Growth Stimulation

(A) PLK1-mediated phosphorylation of KIF2A at T554 in vitro was probed by western blotting with the anti-phospho-KIF2A (T554) rabbit polyclonal antibody. The loading levels of His-PLK1 and GST-tagged KIF2A proteins were also detected by western blotting.

(B–D) After 24 hr serum starvation, hTERT-RPE1 cells were stimulated with 10% serum for 4 hr in the presence or absence of 100 nM BI2536 and then immunostained with anti-ninein (red), anti-acetylated tubulin (blue), and anti-KIF2A (B); anti-phospho-T554-KIF2A (C); or anti-phospho-T210 PLK1 (D) (green) antibodies. In the presence of 100 nM BI2536, the phospho-T554-KIF2A and phospho-T210-PLK1 signals at the mother centriole were rarely detected at 4 hr post-serum stimulation. The scale bar represents 2 μm.

(E) hTERT-RPE1 cells were transfected with AcGFP1-tagged KIF2A, PLK1 phosphorylation mimic KIF2A mutant (T554E), or KIF2A T554E mutant with KEC/KVD motif double mutations and cultured without serum for 24 hr in the presence or absence of 100 nM BI2536 before immunostaining with anti-GFP (green) and anti-acetylated-tubulin (red) antibodies. DNA was stained with DAPI (blue). Arrow indicates the centrosome/basal body. The scale bar represents 10 μm.

(F) Percentage of cells with primary cilia in GFP-positive cells from (E). The phospho-mimic T554E KIF2A mutant significantly inhibited ciliogenesis even in the presence of 100 nM BI2536. KEC/KVD motif mutations of KIF2A abrogated the T554E enhancement of primary cilia disassembly (means ± SD; ***$p < 0.001$; t test; n = 3; >200 cells per experiment).

OPEN ACCESS
CellPress

Please cite this article in press as: Miyamoto et al., The Microtubule-Depolymerizing Activity of a Mitotic Kinesin Protein KIF2A Drives Primary Cilia Disassembly Coupled with Cell Proliferation, Cell Reports (2015), http://dx.doi.org/10.1016/j.celrep.2015.01.003

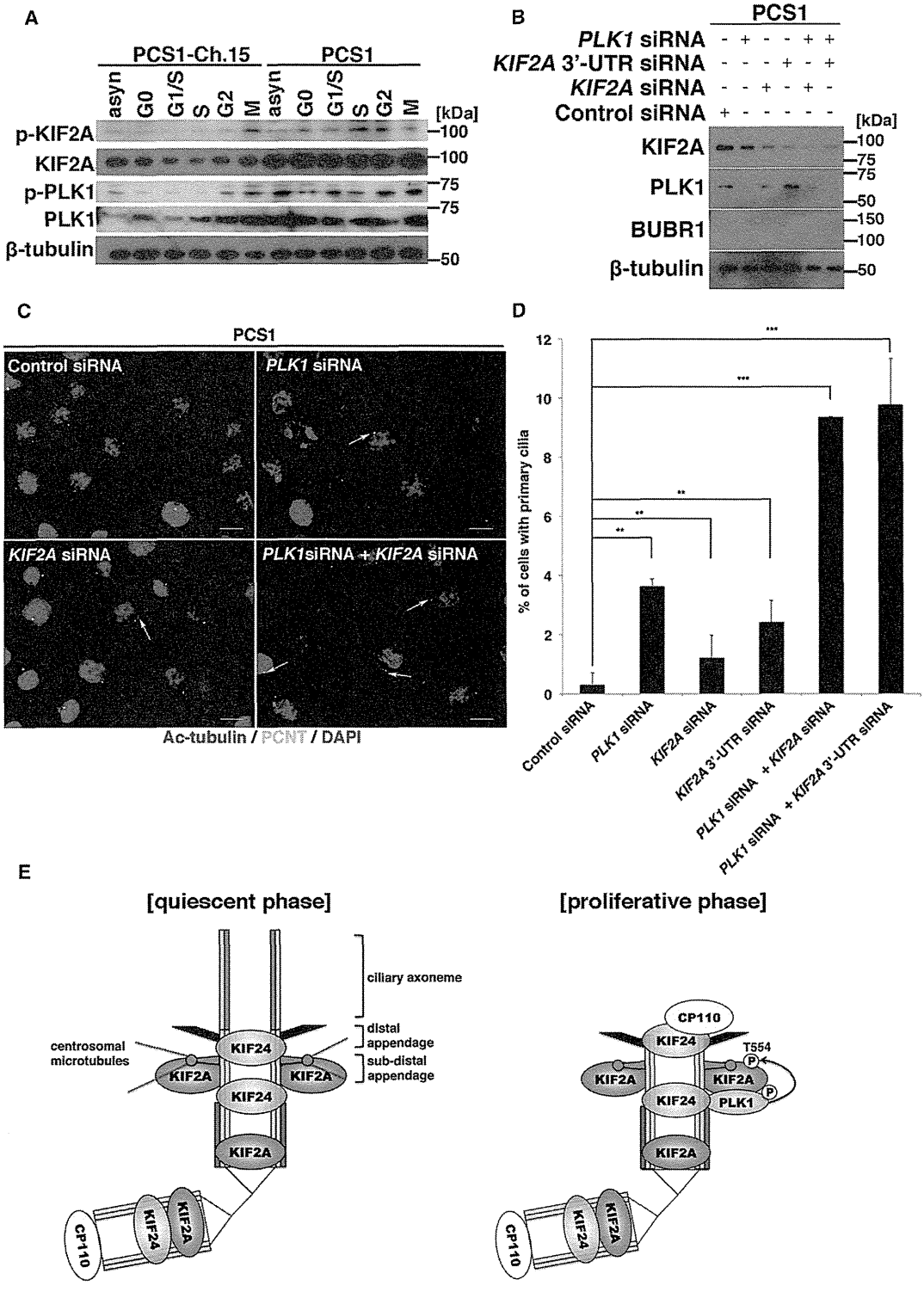

Figure 4. Inhibition of the PLK1-KIF2A Pathway Rescues Ciliogenesis in PCS Syndrome

(A) Phosphorylation levels of PLK1 (T210) and KIF2A (T554) during the cell cycle in immortalized fibroblast cells from a patient (PCS1) with PCS (MVA) syndrome and PCS1 cells transferred with a whole chromosome 15 containing the *BUB1B* locus (PCS1-Ch.15 cells) were analyzed by western blotting.

(B) siRNA-mediated knockdown of *PLK1* and/or *KIF2A* in PCS1 cells was evaluated by western blotting. β-tubulin served as a loading control.

(legend continued on next page)

patient cells had an aberrant activation of PLK1 throughout the cell cycle (Figure 4A). In this study, we found an additional pathological mechanism of impaired ciliogenesis in PCS (MVA) syndrome. Our data demonstrated that the aberrant PLK1-KIF2A pathway contributes to the ciliopathy disease spectrum in PCS (MVA) syndrome.

In conclusion, we demonstrate that the PLK1-KIF2A pathway is essential for primary cilia disassembly induced by growth signals and that constitutive activation of this pathway is responsible for the defective ciliogenesis of the PCS (MVA) syndrome.

EXPERIMENTAL PROCEDURES

Cell Culture

hTERT-RPE1, HEK293T, an immortalized fibroblast cell line from a patient with the PCS (MVA) syndrome (PCS1; Matsuura et al., 2006; Miyamoto et al., 2011), and chromosome-15-transferred PCS1 cells (PCS1-Ch.15) (Matsuura et al., 2006; Miyamoto et al., 2011) were maintained in DMEM supplemented with 10% fetal bovine serum at 37°C with 5% CO_2. Transfection of plasmids or siRNAs into cells was performed using Lipofectamine LTX reagent (Life Technologies) or Lipofectamine RNAi MAX reagent (Life Technologies), respectively, according to the manufacturer's protocol. At 24 hr after transfection, the medium was replaced with serum-free DMEM and the cells were incubated for 24 hr to become Ki-67-negative and achieve quiescent G0 phase to observe ciliogenesis. To avoid the possibility of ciliogenesis induced by contact inhibition, cells were maintained at <100% confluence in all experiments. Cell-cycle profile was analyzed with Muse Cell Analyzer (Millipore).

Detailed experimental procedures are included in the Supplemental Experimental Procedures.

SUPPLEMENTAL INFORMATION

Supplemental Information includes Supplemental Experimental Procedures and four figures and can be found with this article online at http://dx.doi.org/10.1016/j.celrep.2015.01.003.

ACKNOWLEDGMENTS

We thank Drs. A. Inoko and Y. Saito for critical reading and helpful discussions. We also thank Dr. H. Hosoya for technical support and Ms. Y. Tonouchi for assistance. This work was supported by a Grant-in-Aid for Scientific Research from the Ministry of Education, Culture, Sports, Science and Technology of Japan (to S.M. and T.M.); a Grant-in-Aid for Scientific Research from the Ministry of Health, Labour and Welfare (to S.M.); research grants from Naito Foundation (to S.M.), Takeda Science Foundation (to T.M.), and Tsuchiya Medical Foundation (to T.M.); a research grant from Platform for Dynamic Approach to Living Systems from the Ministry of Education, Culture, Sports, Science and Technology, Japan (to H.O.); and an NIH grant R01HD069647 (to B.D.D.).

Received: July 2, 2014
Revised: December 9, 2014
Accepted: December 24, 2014
Published: February 5, 2015

REFERENCES

Bhogaraju, S., Cajanek, L., Fort, C., Blisnick, T., Weber, K., Taschner, M., Mizuno, N., Lamla, S., Bastin, P., Nigg, E.A., and Lorentzen, E. (2013). Molecular basis of tubulin transport within the cilium by IFT74 and IFT81. Science *341*, 1009–1012.

Blaineau, C., Tessier, M., Dubessay, P., Tasse, L., Crobu, L., Pagès, M., and Bastien, P. (2007). A novel microtubule-depolymerizing kinesin involved in length control of a eukaryotic flagellum. Curr. Biol. *17*, 778–782.

Bruinsma, W., Raaijmakers, J.A., and Medema, R.H. (2012). Switching Polo-like kinase-1 on and off in time and space. Trends Biochem. Sci. *37*, 534–542.

Dawson, S.C., Sagolla, M.S., Mancuso, J.J., Woessner, D.J., House, S.A., Fritz-Laylin, L., and Cande, W.Z. (2007). Kinesin-13 regulates flagellar, interphase, and mitotic microtubule dynamics in Giardia intestinalis. Eukaryot. Cell *6*, 2354–2364.

Ganem, N.J., and Compton, D.A. (2004). The KinI kinesin Kif2a is required for bipolar spindle assembly through a functional relationship with MCAK. J. Cell Biol. *166*, 473–478.

Ganner, A., Lienkamp, S., Schäfer, T., Romaker, D., Wegierski, T., Park, T.J., Spreitzer, S., Simons, M., Gloy, J., Kim, E., et al. (2009). Regulation of ciliary polarity by the APC/C. Proc. Natl. Acad. Sci. USA *106*, 17799–17804.

Hanks, S., Coleman, K., Reid, S., Plaja, A., Firth, H., Fitzpatrick, D., Kidd, A., Méhes, K., Nash, R., Robin, N., et al. (2004). Constitutional aneuploidy and cancer predisposition caused by biallelic mutations in BUB1B. Nat. Genet. *36*, 1159–1161.

Homma, N., Takei, Y., Tanaka, Y., Nakata, T., Terada, S., Kikkawa, M., Noda, Y., and Hirokawa, N. (2003). Kinesin superfamily protein 2A (KIF2A) functions in suppression of collateral branch extension. Cell *114*, 229–239.

Hood, E.A., Kettenbach, A.N., Gerber, S.A., and Compton, D.A. (2012). Plk1 regulates the kinesin-13 protein Kif2b to promote faithful chromosome segregation. Mol. Biol. Cell *23*, 2264–2274.

Ishikawa, H., and Marshall, W.F. (2011). Ciliogenesis: building the cell's antenna. Nat. Rev. Mol. Cell Biol. *12*, 222–234.

Izumi, H., Matsumoto, Y., Ikeuchi, T., Saya, H., Kajii, T., and Matsuura, S. (2009). BubR1 localizes to centrosomes and suppresses centrosome amplification via regulating Plk1 activity in interphase cells. Oncogene *28*, 2806–2820.

Jang, C.Y., Coppinger, J.A., Seki, A., Yates, J.R., 3rd, and Fang, G. (2009). Plk1 and Aurora A regulate the depolymerase activity and the cellular localization of Kif2a. J. Cell Sci. *122*, 1334–1341.

Kobayashi, T., and Dynlacht, B.D. (2011). Regulating the transition from centriole to basal body. J. Cell Biol. *193*, 435–444.

Kobayashi, T., Tsang, W.Y., Li, J., Lane, W., and Dynlacht, B.D. (2011). Centriolar kinesin Kif24 interacts with CP110 to remodel microtubules and regulate ciliogenesis. Cell *145*, 914–925.

Lee, K.H., Johmura, Y., Yu, L.R., Park, J.E., Gao, Y., Bang, J.K., Zhou, M., Veenstra, T.D., Yeon Kim, B., and Lee, K.S. (2012). Identification of a novel Wnt5a-CK1ε-Dvl2-Plk1-mediated primary cilia disassembly pathway. EMBO J. *31*, 3104–3117.

Maor-Nof, M., Homma, N., Raanan, C., Nof, A., Hirokawa, N., and Yaron, A. (2013). Axonal pruning is actively regulated by the microtubule-destabilizing protein kinesin superfamily protein 2A. Cell Rep. *3*, 971–977.

(C) PCS1 cells transfected with control siRNA, *PLK1* siRNA, *KIF2A* siRNA, or a combination of *PLK1* siRNA and *KIF2A* siRNA were cultured without serum for 24 hr and then immunostained with anti-acetylated tubulin (red) and anti-pericentrin (green) antibodies. DNA was stained with DAPI (blue). Arrows indicate primary cilia. The scale bar represents 10 μm.

(D) Quantification of the percentage of ciliated cells from (C). Knockdown of PLK1 and/or KIF2A in PCS1 cells significantly restored ciliogenesis (means ± SD; $^{**}p < 0.01$; $^{***}p < 0.001$; t test; n = 3; >200 cells per experiment).

(E) Model for the physiological activation of the PLK1-KIF2A pathway in the context of primary cilia disassembly activated by cell-cycle re-entry. During the proliferative phase, KIF2A phosphorylated at T554 by PLK1 enhances the MT disassembly at the subdistal appendage for primary cilia disassembly, whereas KIF24 at the more-distal end than the subdistal appendage recruits CP110 to prevent inappropriate ciliogenesis (Tsang and Dynlacht, 2013). In the pathological context of PCS (MVA) syndrome, germline mutations of *BUB1B* gene encoding BUBR1 causes the constitutive activation of the PLK1-KIF2A pathway to impair ciliogenesis. See also Figures S2–S4.

Please cite this article in press as: Miyamoto et al., The Microtubule-Depolymerizing Activity of a Mitotic Kinesin Protein KIF2A Drives Primary Cilia Disassembly Coupled with Cell Proliferation, Cell Reports (2015), http://dx.doi.org/10.1016/j.celrep.2015.01.003

Matsuura, S., Matsumoto, Y., Morishima, K., Izumi, H., Matsumoto, H., Ito, E., Tsutsui, K., Kobayashi, J., Tauchi, H., Kajiwara, Y., et al. (2006). Monoallelic BUB1B mutations and defective mitotic-spindle checkpoint in seven families with premature chromatid separation (PCS) syndrome. Am. J. Med. Genet. A. *140*, 358–367.

Miyamoto, T., Porazinski, S., Wang, H., Borovina, A., Ciruna, B., Shimizu, A., Kajii, T., Kikuchi, A., Furutani-Seiki, M., and Matsuura, S. (2011). Insufficiency of BUBR1, a mitotic spindle checkpoint regulator, causes impaired ciliogenesis in vertebrates. Hum. Mol. Genet. *20*, 2058–2070.

Nakajima, H., Toyoshima-Morimoto, F., Taniguchi, E., and Nishida, E. (2003). Identification of a consensus motif for Plk (Polo-like kinase) phosphorylation reveals Myt1 as a Plk1 substrate. J. Biol. Chem. *278*, 25277–25280.

Nigg, E.A., and Raff, J.W. (2009). Centrioles, centrosomes, and cilia in health and disease. Cell *139*, 663–678.

Nigg, E.A., and Stearns, T. (2011). The centrosome cycle: Centriole biogenesis, duplication and inherent asymmetries. Nat. Cell Biol. *13*, 1154–1160.

Peters, J.M. (2006). The anaphase promoting complex/cyclosome: a machine designed to destroy. Nat. Rev. Mol. Cell Biol. *7*, 644–656.

Piao, T., Luo, M., Wang, L., Guo, Y., Li, D., Li, P., Snell, W.J., and Pan, J. (2009). A microtubule depolymerizing kinesin functions during both flagellar disassembly and flagellar assembly in Chlamydomonas. Proc. Natl. Acad. Sci. USA *106*, 4713–4718.

Seeger-Nukpezah, T., Liebau, M.C., Höpker, K., Lamkemeyer, T., Benzing, T., Golemis, E.A., and Schermer, B. (2012). The centrosomal kinase Plk1 localizes to the transition zone of primary cilia and induces phosphorylation of nephrocystin-1. PLoS ONE *7*, e38838.

Sharma, N., Kosan, Z.A., Stallworth, J.E., Berbari, N.F., and Yoder, B.K. (2011). Soluble levels of cytosolic tubulin regulate ciliary length control. Mol. Biol. Cell *22*, 806–816.

Tateishi, K., Yamazaki, Y., Nishida, T., Watanabe, S., Kunimoto, K., Ishikawa, H., and Tsukita, S. (2013). Two appendages homologous between basal bodies and centrioles are formed using distinct Odf2 domains. J. Cell Biol. *203*, 417–425.

Tsang, W.Y., and Dynlacht, B.D. (2013). CP110 and its network of partners coordinately regulate cilia assembly. Cilia *2*, 9.

Tucker, R.W., Pardee, A.B., and Fujiwara, K. (1979). Centriole ciliation is related to quiescence and DNA synthesis in 3T3 cells. Cell *17*, 527–535.

Walczak, C.E., Gayek, S., and Ohi, R. (2013). Microtubule-depolymerizing kinesins. Annu. Rev. Cell Dev. Biol. *29*, 417–441.

Wang, G., Chen, Q., Zhang, X., Zhang, B., Zhuo, X., Liu, J., Jiang, Q., and Zhang, C. (2013a). PCM1 recruits Plk1 to the pericentriolar matrix to promote primary cilia disassembly before mitotic entry. J. Cell Sci. *126*, 1355–1365.

Wang, L., Piao, T., Cao, M., Qin, T., Huang, L., Deng, H., Mao, T., and Pan, J. (2013b). Flagellar regeneration requires cytoplasmic microtubule depolymerization and kinesin-13. J. Cell Sci. *126*, 1531–1540.

Wang, W., Wu, T., and Kirschner, M.W. (2014). The master cell cycle regulator APC-Cdc20 regulates ciliary length and disassembly of the primary cilium. eLife *3*, e03083.

Zhang, L., Shao, H., Huang, Y., Yan, F., Chu, Y., Hou, H., Zhu, M., Fu, C., Aikhionbare, F., Fang, G., et al. (2011). PLK1 phosphorylates mitotic centromere-associated kinesin and promotes its depolymerase activity. J. Biol. Chem. *286*, 3033–3046.

ORIGINAL RESEARCH ARTICLE | Genetics inMedicine

Open

Comprehensive and quantitative multilocus methylation analysis reveals the susceptibility of specific imprinted differentially methylated regions to aberrant methylation in Beckwith–Wiedemann syndrome with epimutations

Toshiyuki Maeda, MD[1,2], Ken Higashimoto, PhD[1], Kosuke Jozaki, PhD[1], Hitomi Yatsuki, PhD[1], Kazuhiko Nakabayashi, PhD[3], Yoshio Makita, PhD[4], Hidefumi Tonoki, PhD[5], Nobuhiko Okamoto, MD[6], Fumio Takada, PhD[7], Hirofumi Ohashi, PhD[8], Makoto Migita, PhD[9], Rika Kosaki, MD[10], Keiko Matsubara, PhD[11], Tsutomu Ogata, PhD[12], Muneaki Matsuo, PhD[2], Yuhei Hamasaki, PhD[2], Yasufumi Ohtsuka, MD[1,2], Kenichi Nishioka, PhD[1], Keiichiro Joh, PhD[1], Tsunehiro Mukai, PhD[13], Kenichiro Hata, PhD[3] and Hidenobu Soejima, PhD[1]

Purpose: Expression of imprinted genes is regulated by DNA methylation of differentially methylated regions (DMRs). Beckwith–Wiedemann syndrome is an imprinting disorder caused by epimutations of DMRs at 11p15.5. To date, multiple methylation defects have been reported in Beckwith–Wiedemann syndrome patients with epimutations; however, limited numbers of DMRs have been analyzed. The susceptibility of DMRs to aberrant methylation, alteration of gene expression due to aberrant methylation, and causative factors for multiple methylation defects remain undetermined.

Methods: Comprehensive methylation analysis with two quantitative methods, matrix-assisted laser desorption/ionization mass spectrometry and bisulfite pyrosequencing, was conducted across 29 DMRs in 54 Beckwith–Wiedemann syndrome patients with epimutations. Allelic expressions of three genes with aberrant methylation were analyzed. All DMRs with aberrant methylation were sequenced.

Results: Thirty-four percent of *Kv*DMR1–loss of methylation patients and 30% of *H19*DMR–gain of methylation patients showed multiple methylation defects. Maternally methylated DMRs were susceptible to aberrant hypomethylation in *Kv*DMR1–loss of methylation patients. Biallelic expression of the genes was associated with aberrant methylation. *Cis*-acting pathological variations were not found in any aberrantly methylated DMR.

Conclusion: Maternally methylated DMRs may be vulnerable to DNA demethylation during the preimplantation stage, when hypomethylation of *Kv*DMR1 occurs, and aberrant methylation of DMRs affects imprinted gene expression. *Cis*-acting variations of the DMRs are not involved in the multiple methylation defects.

Genet Med advance online publication 8 May 2014

Key Words: Beckwith–Wiedemann syndrome; DNA methylation; differentially methylated region; genomic imprinting; multiple methylation defects

INTRODUCTION

Genomic imprinting is an epigenetic phenomenon that leads to parent-specific differential expression of a subset of mammalian genes. Most imprinted genes are clustered in regions called imprinting domains, and the expression of imprinted genes within these domains is regulated by imprinting control regions.[1,2] Differentially methylated regions (DMRs), which are defined as having DNA methylation on only one of the two parental alleles, play critical roles in the regulation of imprinting. There are two kinds of DMRs: maternally methylated DMRs (matDMRs) and paternally methylated DMRs (patDMRs). In addition, there is another classification, gametic DMRs and somatic DMRs, based on the timing of the establishment of differential methylation. Gametic DMRs acquire DNA methylation during gametogenesis, and the methylation is maintained from zygote to somatic cells during all developmental stages. Most gametic DMRs are identical to imprinting control regions. On the other hand, somatic DMRs are established during early embryogenesis after fertilization under the control of nearby imprinting control regions.[1,2] Because imprinted genes play an important role in the growth and development of embryos, placental formation, and metabolism, aberrant expression of

[1]Division of Molecular Genetics and Epigenetics, Department of Biomolecular Sciences, Faculty of Medicine, Saga University, Saga, Japan; [2]Department of Pediatrics, Faculty of Medicine, Saga University, Saga, Japan; [3]Department of Maternal–Fetal Biology, National Research Institute for Child Health and Development, Tokyo, Japan; [4]Education Center, Asahikawa Medical University, Asahikawa, Japan; [5]Department of Pediatrics, Maternal, Perinatal, and Child Medical Center, Tenshi Hospital, Sapporo, Japan; [6]Department of Medical Genetics, Osaka Medical Center and Research Institute for Maternal and Child Health, Izumi, Japan; [7]Department of Medical Genetics, Kitasato University Graduate School of Medical Sciences, Kanagawa, Japan; [8]Division of Medical Genetics, Saitama Children's Medical Center, Saitama, Japan; [9]Department of Pediatrics, Nippon Medical School, Tokyo, Japan; [10]Division of Medical Genetics, National Center for Child Health and Development, Tokyo, Japan; [11]Department of Molecular Endocrinology, National Research Institute for Child Health and Development, Tokyo, Japan; [12]Department of Pediatrics, Hamamatsu University School of Medicine, Hamamatsu, Japan; [13]Nishikyushu University, Saga, Japan. Correspondence: Hidenobu Soejima (soejimah@cc.saga-u.ac.jp)

Submitted 10 November 2013; accepted 7 April 2014; advance online publication 8 May 2014. doi:10.1038/gim.2014.46

imprinted genes due to epigenetic or genetic abnormalities is implicated in the pathogenesis of some human disorders, such as congenital anomalies and tumors.[1,2]

Beckwith–Wiedemann syndrome (BWS; Online Mendelian Inheritance in Man (OMIM) #130650) is an imprinting disease that is characterized by prenatal and postnatal macrosomia, macroglossia, abdominal wall defects, and variable minor features. The relevant imprinted chromosomal region in BWS is 11p15.5, which consists of two imprinted domains, *IGF2/H19* and *CDKN1C/KCNQ1OT1*, *H19*DMR and *Kv*DMR1 being the respective imprinting control regions.[3–5] Among several causative alterations identified so far, loss of methylation (LOM) at *Kv*DMR1 and gain of methylation (GOM) at *H19*DMR are isolated epimutations. Hypomethylation at multiple imprinted DMRs has been reported in patients with transient neonatal diabetes mellitus type 1,[6] and the same phenomenon, referred to as multiple methylation defects (MMDs), has been reported in BWS patients with *Kv*DMR1-LOM.[7–13] However, although the human genome contains more than 30 imprinting domains (http://www.geneimprint.com), a limited number of imprinted DMRs have been analyzed so far, with the exception of a report by Court et al.[12] In addition, methods used for methylation analysis have ranged from nonquantitative to quantitative approaches, and although some studies have used only one method for methylation analysis,[8,9,11] others have used two or more in conjuction.[7,10–13] Furthermore, the questions of whether susceptibility to aberrant methylation is different in each type of DMR, whether aberrant methylation indeed affects imprinted gene expression, and what causative factors are responsible for MMDs still remain unanswered. To clarify these issues, we have conducted a comprehensive methylation screening in BWS patients with *Kv*DMR1-LOM or *H19*DMR-GOM with a quantitative method, matrix-assisted laser desorption/ionization mass spectrometry (MALDI-TOF MS), on 29 imprinted DMRs, which represents the largest number of DMRs analyzed to date, followed by confirmation with another quantitative method, bisulfite pyrosequencing. We also performed gene expression analysis and sequencing of aberrantly methylated DMRs. We found that matDMRs are susceptible to aberrant methylation. We also found alterations in imprinted gene expression due to the aberrant methylation and no *cis*-acting pathological variations in DMRs with MMDs.

MATERIALS AND METHODS

Patients

Fifty-four BWS patients (25 boys, 26 girls, 3 gender-unspecified patients; average age: 3.0 years (0–13.9 years)) and their parents were enrolled in this study. Among them, 46 patients met clinical criteria for BWS as described by Weksberg et al.[3] and 6 patients met clinical criteria as described by DeBaun et al.[14] (**Supplementary Table S1** online). Because two patients were clinically diagnosed more than 20 years ago, their specific diagnostic criteria were unknown. The methylation statuses of *H19*DMR and *Kv*DMR1, paternal uniparental disomy of chromosome 11 (upd(11)pat), and *CDKN1C* mutations were screened as described previously.[15–17] Peripheral blood samples of most patients were subjected to standard G-banding chromosome analysis and/or high-resolution G-band patterning of human chromosome 11, but neither assay showed any abnormalities in any patient (data not shown). Among the 54 patients, 44 displayed *Kv*DMR1-LOM but did not show other causative alterations, including *H19*DMR-GOM, upd(11)pat, and *CDKN1C* mutations (data not shown). The remaining 10 patients displayed *H19*DMR-GOM but did not show other causative alterations (data not shown). We sequenced the entire *H19*DMR in *H19*DMR-GOM patients and found no mutations.[18] We used the peripheral blood samples of 24 children (11 boys, 13 girls; average age: 3.8 years (range of 0–8 years)) who visited the Department of Pediatrics, Saga University Hospital, as normal controls having only mild illness such as common cold. This study was approved by the Ethics Committee for Human Genome and Gene Analyses of the Faculty of Medicine, Saga University. Written informed consent was obtained from the parents or the guardians of the patients and participants.

DNA isolation and bisulfite conversion

Genomic DNA was extracted from the peripheral blood of patients using the FlexiGene DNA Kit (Qiagen, Hilden, Germany) according to the manufacturer's instructions. A total of 1 μg of genomic DNA was subjected to bisulfite conversion using the EZ DNA Methylation Kit (Zymo Research, Irvine, CA), and then the converted DNA was eluted in 100 μl of water. Unmethylated control DNA was created by whole-genome amplification using the REPLI-g Mini Kit (Qiagen). To prepare fully methylated control DNA, the unmethylated DNA created by whole-genome amplification was treated twice with *Sss*I methylase.

Methylation analysis by MALDI-TOF MS

The DNA methylation status of imprinted DMRs was analyzed by MALDI-TOF MS analysis with a MassARRAY system (Sequenom, San Diego, CA) as previously described.[19,20] Briefly, each DMR was amplified by bisulfite-mediated polymerase chain reaction (PCR) using a primer set containing a primer carrying the T7 promoter sequence at the 5′ end. In vitro transcription of the PCR product was performed with T7 RNA polymerase, and the transcript was subjected to uracil-specific cleavage with RNase A. MALDI-TOF MS analysis of the cleaved fragments produced signal pattern pairs indicative of nonmethylated and methylated DNA. Epityper software (Sequenom) analysis of the signals yielded a methylation index (MI) ranging from 0 (no methylation) to 1 (full methylation) for each CpG unit, which contained one or more CpG sites. Aberrant methylation of a CpG unit was defined as the condition in which the difference of MIs between each patient and the average of normal controls exceeded 0.15. This definition was based on our finding in methylation-sensitive Southern blots, which revealed that the differences in MI for *Kv*DMR1-LOM or *H19*DMR-GOM in BWS patients were ≥0.15 (data not shown). Because the analyzed DMRs included several CpG units, aberrant methylation of each DMR was defined as the situation in which more

than 60% of the total number of analyzed CpG units showed aberrant methylation (with the MI difference exceeding 0.15). In the case of *IGF2*-DMR0, the three CpG sites were analyzed based on previous reports.[21,22] All primers used in this study are shown in **Supplementary Table S2** online.

Methylation analysis by bisulfite pyrosequencing

The aberrant methylation status of DMRs identified by MALDI-TOF MS was confirmed by bisulfite pyrosequencing using QIAGEN PyroMark Q24 according to the manufacturer's instructions (Qiagen). Primers for bisulfite-mediated PCR and pyrosequencing were designed using PyroMark Assay Design 2.0 (Qiagen). In analogy with MALDI-TOF MS analysis, aberrant methylation of a CpG site was defined as the situation in which the difference of MIs between each patient and the average of normal controls exceeded 0.15. Aberrant methylation of each DMR was defined as the condition in which more than 60% of the total number of analyzed CpG sites showed aberrant methylation (with the MI difference exceeding 0.15).

Bisulfite sequencing

Bisulfite sequencing was performed to analyze allelic methylation of *ZDBF2*-DMR. After PCR amplification, the PCR products were cloned into a pT7Blue T-Vector (Novagen, Darmstadt, Germany), and individual clones were sequenced. Parental alleles were distinguished by a single-nucleotide polymorphism (SNP, *rs1861437*) within the DMR.

Expression analysis of *ZDBF2*, *FAM50B*, and *GNAS1A*

Total RNA was extracted from the peripheral blood of patients using the QIAamp RNA Blood Mini Kit (Qiagen). The RNA was treated with RNase-free DNase I, and reverse transcription was performed with random primers. We used SNPs for allelic expression to distinguish between the two parental alleles: *rs10932150* in exon 5 of *ZDBF2*; *rs6597007* in exon 2 of *FAM50B*; and *rs143800311*, which is a 5-bp deletion/insertion variation in exon 1A of *GNAS1A*. Reverse transcription–PCR (RT-PCR) products encompassing the SNPs of *ZDBF2* and *FAM50B* were directly sequenced. The products encompassing the deletion/insertion variation of *GNAS1A* were separated by electrophoresis on an Applied Biosystems 3130 genetic analyzer (Applied Biosystems, Foster City, CA) and then analyzed with GeneMapper software (Applied Biosystems). Total expression levels of *ZDBF2* and *FAM50B* were quantitated by real-time PCR with TaqMan probes (Applied Biosystems). The expression level of each gene was normalized against that of the housekeeping genes encoding hydroxymethylbilane synthase (*HMBS*) and glyceraldehyde-3-phosphate dehydrogenase (*GAPDH*). All quantitative RT-PCRs were performed in triplicate.

Sequencing of aberrantly methylated DMRs

Direct sequencing of all DMRs showing aberrant methylation in *Kv*DMR1-LOM patients was performed to determine whether there was any pathological variation.

Statistical analyses

Fisher's exact test was used for the comparison of aberrant methylated DMRs. Fisher's exact test or Mann–Whitney *U*-test was used for statistical analyses of clinical features between MMDs and monolocus methylation defects in *Kv*DMR1-LOM patients. A P value < 0.05 was considered statistically significant.

RESULTS

Validation of methylation analyses, MALDI-TOF MS, and bisulfite pyrosequencing

First, we selected 37 regions reported previously as imprinted DMRs in the human genome[16,20,23] (refer to http://www.geneimprint.com/). To validate the quantitative capability of MALDI-TOF MS methylation analysis, mixtures of the unmethylated control DNA and the fully methylated control DNA (0, 25, 50, 75, and 100% methylated DNA) were subjected to bisulfite conversion and analyzed. We found a significant correlation between the measured MIs and predicted MIs in all DMRs, except for *GRB10*, *PEG13*, and IG-DMR-CG4 (**Supplementary Figure S1** online). Furthermore, in normal leukocytes, two regions (*TCEB3C*, *USP29*) showed mostly full methylation and three regions (*TP73*, *SPTBN1*, *WT1-AS*) showed mostly no methylation, suggesting that these regions were not differentially methylated in leukocytes (data not shown). Therefore, we excluded these eight regions and decided to analyze the remaining 29 DMRs by MALDI-TOF MS. Second, we obtained MIs from 24 normal controls using MALDI-TOF MS and calculated the average and SD of each CpG unit. We excluded CpG units in which SDs were >0.1 from further analysis. Averages and SDs of all CpG units analyzed in this study are shown in **Supplementary Table S3** online. After the MALDI-TOF MS analysis, we used bisulfite pyrosequencing to confirm the aberrant methylation uncovered. We also obtained MIs from the 24 controls using bisulfite pyrosequencing and calculated the average and SD of each CpG site. We excluded one CpG site in *H19*DMR because its SD was >0.1 due to a known SNP (*rs10732516*). Averages and SDs of control CpG sites are shown in **Supplementary Table S3** online. Finally, we compared the MIs of MALDI-TOF MS and bisulfite pyrosequencing of each DMR and found a significant correlation (**Supplementary Figure S2** online).

Multilocus methylation defects in BWS patients with epimutations

Among the 44 *Kv*DMR1-LOM patients, 15 (34.1%) showed aberrantly methylated DMRs outside of *Kv*DMR1: six showed aberrant methylation at only one DMR, and the other nine showed two or more methylated DMRs (Figure 1a and **Supplementary Figure S3** online). The greatest number of aberrantly methylated DMRs was found in patient BWS-s113, who exhibited 12 DMRs. Most of the aberrantly methylated DMRs demonstrated LOM, which was seen at *ARHI*-CG1, *ARHI*-CG2, *ARHI*-CG3, *FAM50B*, *ZAC*, *IGF2R*-DMR2, *MEST*, *NNAT*, *L3MBTL1*, *NESPAS*, *GNASXL*, and *GNAS1A*. Among them, the most frequently hypomethylated DMRs were

ARHI-CG1 and *ARHI*-CG3, found in nine (20.5%) and eight (18.2%) patients, respectively. By contrast, three DMRs, located at *ZDBF2*, *NESP*, and *MCTS2*, showed GOM, which was found in six (13.6%), two (4.5%), and one (2.3%) patients, respectively. *GNASXL*-DMR showed GOM in one patient (2.3%), whereas four patients (9.1%) showed LOM. The other 13 DMRs were not aberrantly methylated in any *Kv*DMR1-LOM patient.

Among the 10 *H19*DMR-GOM patients, all patients showed GOM at the *H19* promoter DMR, which was usually observed with loss of imprinting of *IGF2* (Figure 1b).[24] Four patients showed GOM at either *IGF2*-DMR0 or *IGF2*-DMR2; two patients showed GOM at both. Moreover, both LOM and GOM at other DMRs were found: LOM was found at *INPP5Fv2*-DMR in patients BWS-s015 and BWS-s064, and GOM was found at *NESP*-DMR in patient BWS-s012.

In addition, to exclude aberrantly methylated DMRs resulting from chromosome abnormalities such as uniparental disomy and copy number abnormality, microsatellite analyses using patients' and their parents' DNA were performed on all DMRs showing aberrant methylation. For quantitative analyses, tetranucleotide repeat markers near the imprinted DMRs were used (**Supplementary Materials and Methods** online). We found that no DMRs, except for six DMRs in three patients, exhibited any chromosome abnormalities (summarized in **Supplementary Figure S4** online). These results strongly suggest that the aberrant methylation of DMRs observed was

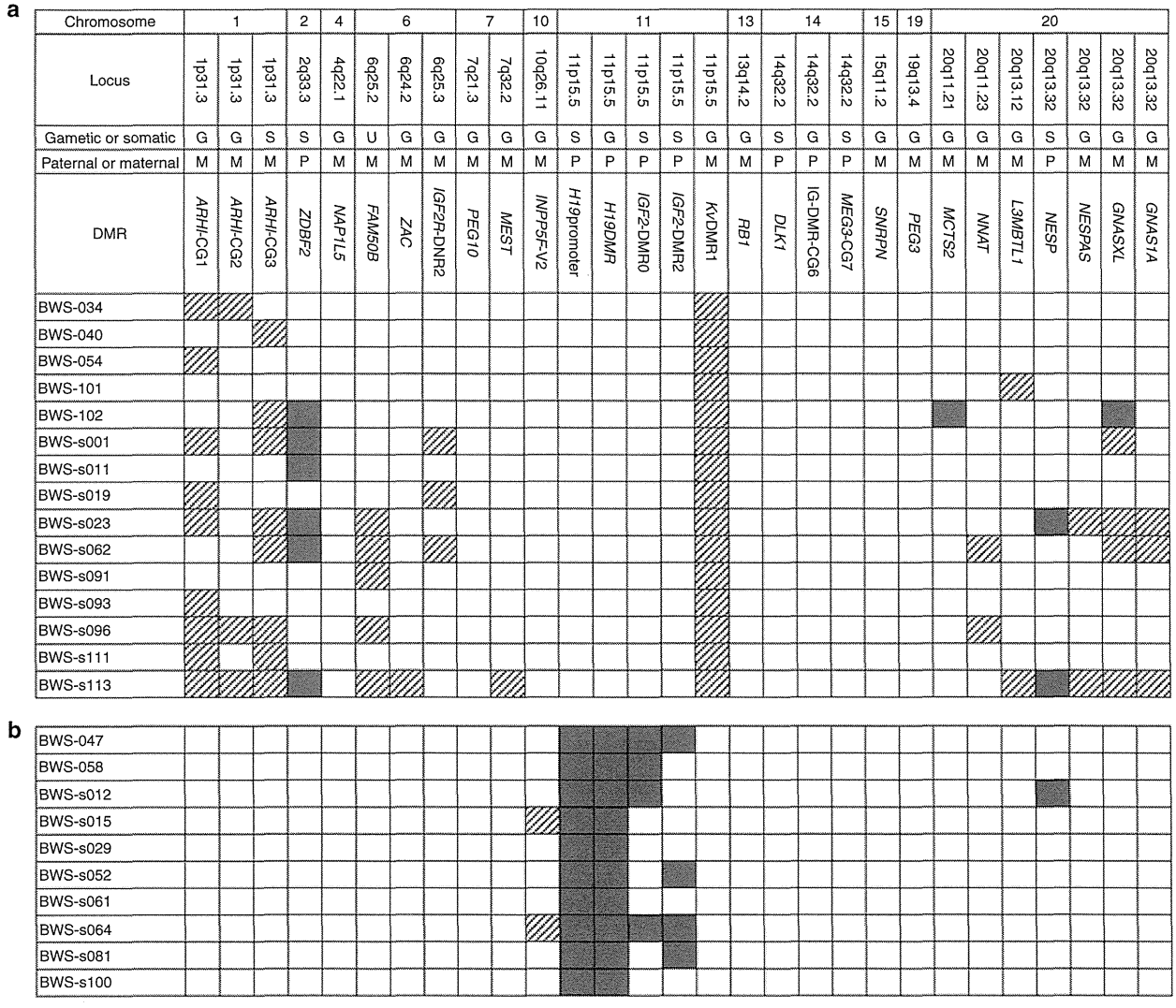

Figure 1 Results of methylation analyses of 29 imprinted differentially methylated regions (DMRs) in Beckwith–Wiedemann syndrome patients with epimutations. (**a**) Results of patients with *Kv*DMR1-LOM. Only the results of multiple methylation defects are shown. Aberrant methylation was confirmed by two quantitative methods: matrix-assisted laser desorption/ionization mass spectrometry and bisulfite pyrosequencing. The definition of aberrant methylation used here is described in the Materials and Methods section. Shaded rectangle: aberrant hypomethylation; dark gray rectangle: aberrant hypermethylation. (**b**) Results of all patients with *H19*DMR-GOM. GOM, gain of methylation; LOM, loss of methylation.

an isolated epimutation and was not due to chromosome abnormalities.

Comparison of aberrantly methylated DMRs

We found that 34.1% (15 of 44) of *Kv*DMR1-LOM patients and 30.0% (3 of 10) of *H19*DMR-GOM patients showed MMDs (Figure 1a). There was no statistical difference between them ($P > 0.99$, Fisher's exact test).

Among the 29 DMRs analyzed, there were 20 gametic DMRs and 8 somatic DMRs (Figure 1a). The timing of methylation establishment of one DMR (*FAM50B*-DMR) has not yet been determined. On the other hand, there were 20 matDMRs and 9 patDMRs. We investigated whether susceptibility to aberrant methylation differed for each type of DMR in *Kv*DMR1-LOM patients. *Kv*DMR1 itself, a gametic and matDMR, was excluded from this analysis. Several DMRs were mapped to certain imprinted domains, e.g., three DMRs in the *ARHI* domain and four in the *GNAS* domain. However, these DMRs differed by type, and aberrant methylations of these DMRs were not always linked. We also had previously found that DMRs in the *GNAS* domain were independently aberrantly methylated in hepatoblastoma.[20] Therefore, we decided to perform statistical analyses assuming the independence of each DMR.

We first compared gametic DMRs with somatic DMRs and found no significant difference in susceptibility ($P = 0.42$, Fisher's exact test; Figure 2a). *FAM50B*-DMR was excluded from this comparison. By contrast, matDMRs were aberrantly methylated more frequently than patDMRs ($P = 0.042$, Fisher's exact test; Figure 2b). In addition, among the aberrantly methylated DMRs, 12 showed LOM and 4 showed GOM. When we compared LOM with GOM, LOM preferentially occurred on matDMRs ($P = 0.050$, Fisher's exact test; Figure 2c). In this subanalysis, *GNASXL*-DMR was counted as having both GOM and LOM (Figure 1a). Furthermore, among the 12 DMRs with LOM, most of them (10) were gametic DMRs. These results suggest that matDMRs are susceptible to aberrant methylation and that gametic maternally methylated DMRs tend to be susceptible to LOM in *Kv*DMR1-LOM patients.

Biallelic expression of imprinted genes induced by aberrant methylation at their corresponding DMRs

We continued our investigation by determining whether allelic expression was associated with the methylation status of the corresponding DMR. We selected three genes (*ZDBF2*, *FAM50B*, and *GNAS1A*) expressed in lymphocytes.[25–27] In the case of *ZDBF2*, bisulfite sequencing of *ZDBF2*-DMR showed paternal monoallelic methylation in normal controls heterozygous for a specific SNP (*rs1861437*), whereas four BWS patients with GOM showed biallelic methylation: these findings were consistent with the results of MALDI-TOF MS and bisulfite pyrosequencing (Figure 3a,b and **Supplementary Figure S5** online). Because paternal expression of the *ZDBF2* gene is coupled with methylation of *ZDBF2*-DMR on the paternal allele,[25] biallelic expression due to biallelic methylation was expected. Indeed, three BWS patients heterozygous for a coding SNP (*rs10932150*) with hypermethylated DMRs clearly showed biallelic expression, in contrast with the paternal monoallelic expression in patients with normally methylated DMRs (Figure 3c). *FAM50B* and *GNAS1A* were paternally expressed and were coupled with maternal methylation of corresponding DMRs. RT-PCR using coding SNPs (*rs6597007* for *FAM50B* and *rs143800311* for *GNAS1A*) revealed that both genes were expressed biallelically with LOM of each corresponding DMR, which was in contrast with monoallelic expression in the patients with normally methylated DMRs (Figure 4 and **Supplementary Figure S5** online). It is intriguing that *FAM50B* in patient BWS-s096 and *GNAS1A* in patient BWS-s062 were expressed from the maternal allele despite low-grade LOM,

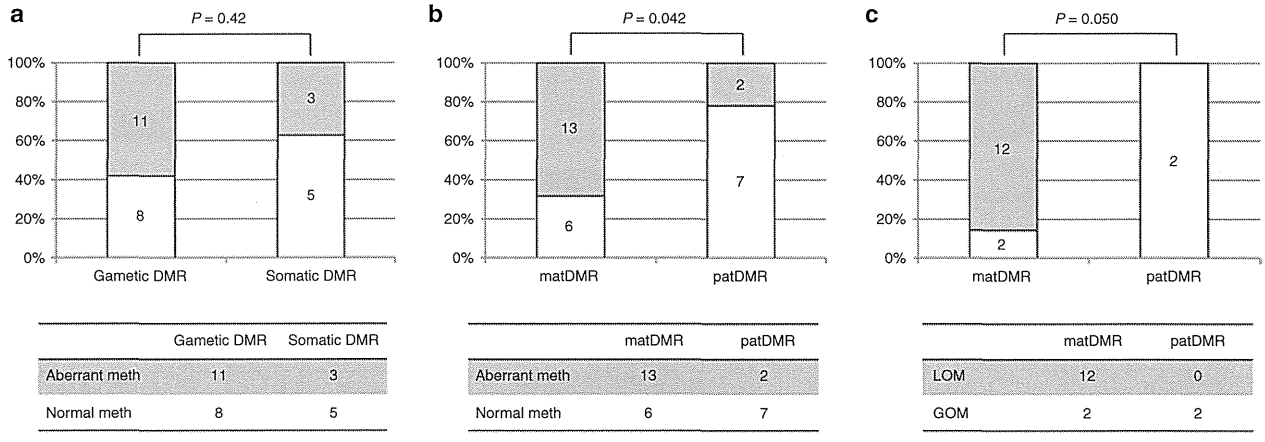

	Gametic DMR	Somatic DMR
Aberrant meth	11	3
Normal meth	8	5

	matDMR	patDMR
Aberrant meth	13	2
Normal meth	6	7

	matDMR	patDMR
LOM	12	0
GOM	2	2

Figure 2 Statistical analyses of aberrantly methylated differentially methylated region (DMRs). (**a**) Comparison of the number of aberrantly methylated DMRs between gametic DMRs and somatic DMRs in *Kv*DMR1-LOM patients. There was no statistical difference between the two DMRs ($P = 0.42$, Fisher's exact test). (**b**) Comparison of the number of aberrantly methylated DMRs between matDMRs and patDMRs in *Kv*DMR1-LOM patients. matDMRs were aberrantly methylated more frequently than patDMRs ($P = 0.042$, Fisher's exact test). (**c**) Comparison of the number of LOMs and GOMs between matDMRs and patDMRs among the aberrantly methylated DMRs in *Kv*DMR1-LOM patients. LOM preferentially occurred on matDMRs ($P = 0.050$, Fisher's exact test). GOM, gain of methylation; LOM, loss of methylation; matDMR, maternally methylated DMR; patDMR, paternally methylated DMR.

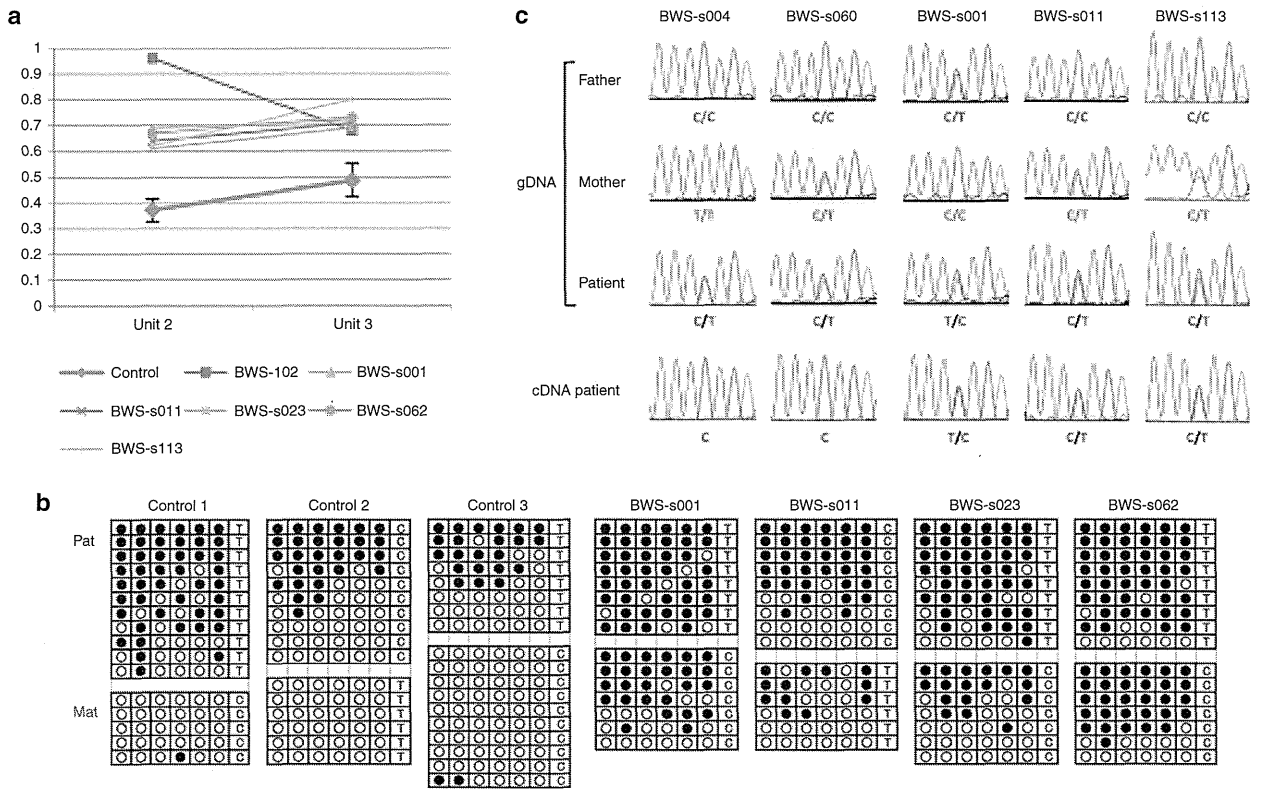

Figure 3 Methylation analysis of *ZDBF2*-DMR and expression analysis of the *ZDBF2* gene. (**a**) Results of matrix-assisted laser desorption/ionization mass spectrometry analysis. Averages with SD of 24 normal controls are shown in blue. Methylation indexes of the patients showing GOM are indicated in different colors. Units 1 and 2 included two and one CpG sites, respectively. (**b**) Results of bisulfite sequencing. Normal controls show monoallelic differential methylation, whereas four Beckwith–Wiedemann syndrome (BWS) patients (BWS-s001, BWS-s011, BWS-s023, and BWS-s060) show biallelic methylation. Two parental alleles were distinguished by a SNP (*rs1861437*). Mat, maternal allele; Pat, paternal allele. (**c**) Results of expression analysis of the *ZDBF2* gene. Three BWS patients (BWS-s001, BWS-s011, and BWS-s113) heterozygous for a coding SNP (*rs10932150*) with GOM clearly showed biallelic expression; by contrast, two patients with normally methylated differentially methylated region (DMRs) exhibited paternal monoallelic expression (patients BWS-s004 and BWS-s060). gDNA, genomic DNA; GOM, gain of methylation; SNP, single-nucleotide polymorphism.

which suggests that our definition of aberrant methylation is appropriate. In addition, we investigated the expression levels of *ZDBF2* and *FAM50B* by quantitative RT-PCR. The expression levels in patients with aberrantly methylated DMRs were higher than those in patients with normally methylated DMRs (**Supplementary Figure S6** online). These results indicate that allelic expression and expression levels were indeed associated with the methylation status of the corresponding DMR in patients with MMDs.

Lack of pathological variation in all aberrantly methylated DMRs in *Kv*DMR1-LOM patients

Because the genetic aberrations of *H19*DMR explained only ~20% of BWS patients with *H19*DMR-GOM,[28] we hypothesized the existence of *cis*-acting variations within aberrantly methylated DMRs. Therefore, we sequenced all aberrantly methylated DMRs, including *Kv*DMR1, in *Kv*DMR1-LOM patients. However, no variations were found in any aberrantly hypomethylated DMRs, except for four known SNPs (summarized in **Supplementary Figure S7** online), suggesting that *cis*-acting pathological variations are not involved in aberrant methylation of these DMRs.

No difference in clinical features between MMDs and monolocus methylation defects

In *Kv*DMR1-LOM patients, there was no significant difference in clinical features between MMDs and monolocus methylation defects, which demonstrated LOM only at *Kv*DMR1 (Table 1). Among 27 patients with *Kv*DMR1-LOM for whom information on conception was available, one patient was conceived using intracytoplasmic sperm injection, two were from artificial insemination by the husband, and two were from ovulation stimulation. We searched for a link between assisted reproductive technology and MMD but could find no relationship (Table 1). The average age of neither the mother nor the father differed between patients with MMDs versus those with monolocus methylation defects (Table 1). The fact that monozygotic twins discordant for BWS were found predominantly for females suggests an insufficient amount of DNA methyltransferase 1 (DNMT1) to maintain *Kv*DMR1 methylation during the overlap in timing

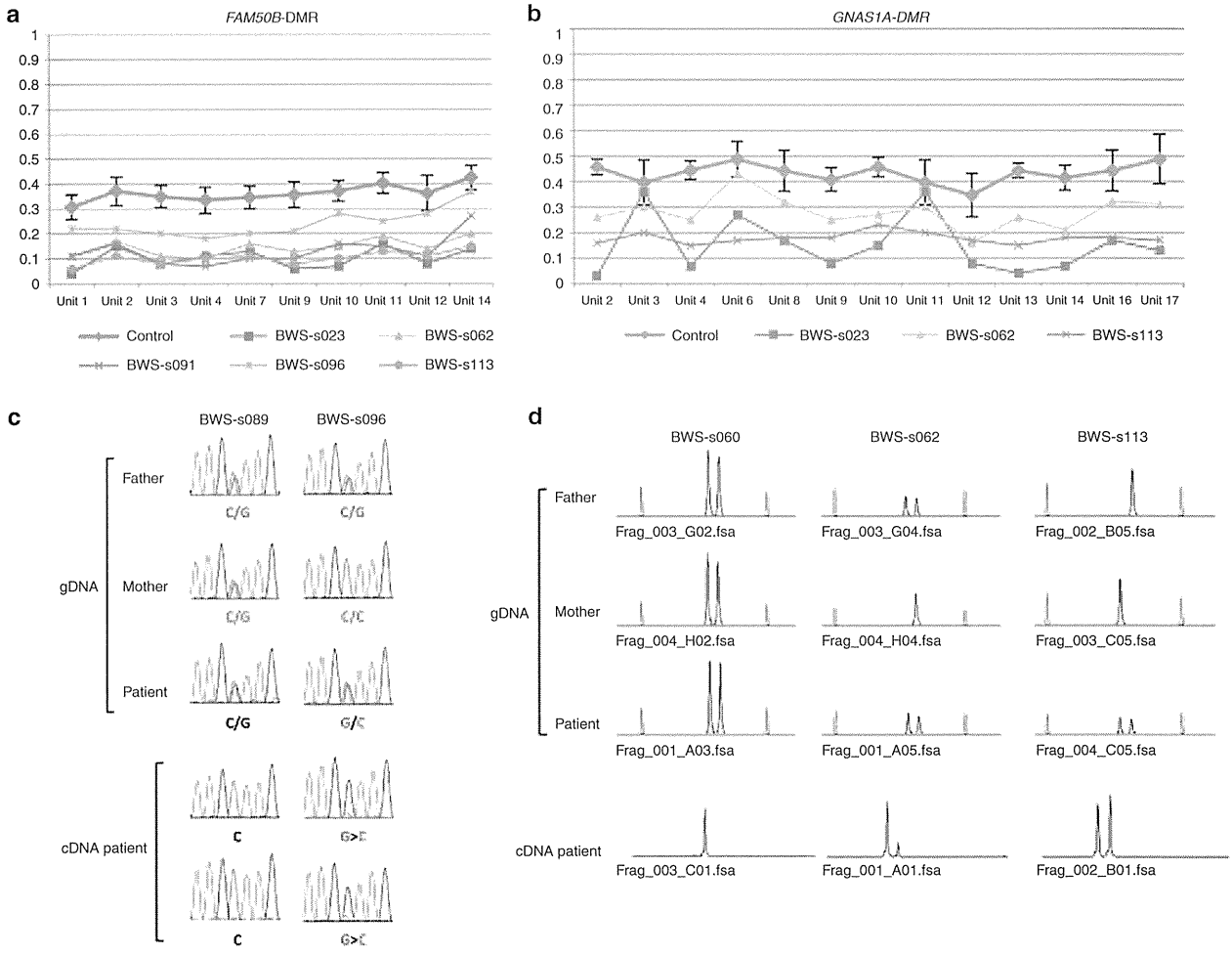

Figure 4 Methylation analysis of *FAM50B*- and *GNAS1A*-DMRs and expression analysis of the *FAM50B* and *GNAS1A* genes. (**a**,**b**) Results of matrix-assisted laser desorption/ionization mass spectrometry analysis. Averages with SD of 24 normal controls are shown in blue. Methylation indexes of patients showing LOM are indicated in different colors. Ten CpG units analyzed for *FAM50B*-DMR covered 13 CpG sites, and 13 CpG units analyzed for *GNAS1A*-DMR covered 18 CpG sites. (**c**) Results of expression analysis of the *FAM50B* gene. Beckwith–Wiedemann syndrome (BWS) patient BWS-s096 was heterozygous for a coding SNP (*rs6597007*) with LOM and showed biallelic expression with a low peak of maternal expression, whereas monoallelic expression was seen in a patient with normally methylated differentially methylated regions (DMRs) (patient BWS-s089). In patient BWS-s096, maternal expression was noted in two independent analyses despite low-grade LOM. gDNA, genomic DNA. (**d**) Results of expression analysis of the *GNAS1A* gene. Patients BWS-s062 and BWS-s113, heterozygous for a deletion/insertion variation (*rs143800311*) with LOM, showed biallelic expression, whereas patient BWS-s060 possessed normally methylated DMRs and exhibited monoallelic expression. Maternal expression was noted despite low-grade LOM in patient BWS-s062. Red peaks are molecular markers. GOM, gain of methylation; LOM, loss of methylation.

with X-chromosome inactivation and twinning.[29] This hypothesis suggests that females might tend to suffer from MMDs. We compared the frequency of female patients with MMDs with the frequency of those with monolocus methylation defects, but no significant difference could be found (Table 1).

DISCUSSION

Currently, most reports have studied 3–10 imprinted DMRs in BWS patients,[7–10,13] with the exception of two reports in which 16 and 27 DMRs were analyzed.[11,12] In addition, the quantitative capability of methods used for multiple methylation analyses has been variable, and few studies have conducted multiple checks to confirm the methylation statuses of all DMRs showing aberrant methylation.[7–13] To resolve these matters, we analyzed 29 DMRs and confirmed all aberrantly methylated DMRs using MALDI-TOF MS and bisulfite pyrosequencing, which are the most reliable quantitative methods of methylation analysis available at present.[19,30,31] We found that 34.1% of *Kv*DMR1-LOM patients exhibited MMDs. The frequency was higher than that in previous reports, which can be summarized as reporting an overall frequency of 20.6% (102 of 495 patients).[7–13] However, within these reports, the frequency in studies that analyzed 10 or fewer DMRs is 19.0% (82 of 431),[7–10,13] and the frequency in studies that analyzed more than 10 DMRs is 31.3% (20 of

Table 1 Clinical features of *Kv*DMR-LOM patients with monolocus methylation defect and those with multilocus methylation defects

	Methylation defect		
	Monolocus	**Multilocus**	***P* value**
Sex			0.22
Male	15	5	
Female	13	9	
Average age of patients	3.3	2.4	0.098[a]
Average age of parents			
Father	31.8	33.8	0.93[a]
Mother	31.8	30.3	0.37[a]
Assisted reproduction technology	3/19 (20%) (AIH 2, OS 1)	2/8 (29%) (ICSI 1, OS 1)	0.47
Standard deviation of average birth weight	+1.9	+2.0	0.58[a]
Overgrowth	21/28 (75%)	9/13 (69%)	0.78
Abdominal wall defect	22/29 (76%)	12/13 (92%)	0.21
Macroglossia	29/29 (100%)	12/12 (100%)	0.60
Hypoglycemia	14/27 (52%)	5/12 (42%)	0.41
Ear pits and creases	19/27 (70.4%)	8/12 (67%)	0.73
Nevus flammeus	9/26 (35%)	4/10 (40%)	0.53
Hemihypertrophy	6/27 (22%)	6/13 (46%)	0.12
Renal anomaly	2/26 (8%)	0/11 (0%)	0.49
Renal enlargement	6/28 (21%)	1/13 (8%)	0.27
Adrenal enlargement	1/27 (4%)	0/11 (0%)	0.71
Hepatomegaly	5/29 (17%)	2/12 (17%)	0.67
Splenomegaly	6/29 (21%)	2/12 (17%)	0.57
Abnormal external genitalia	2/28 (7%)	0/12 (0%)	0.49
Increased bone age	2/15 (13%)	0/3 (0%)	0.69
Cardiac anomaly	2/23 (9%)	0/11 (0%)	0.82
Developmental retardation	6/22 (27%)	0/9 (0%)	0.10
Childhood tumor	5/26 (19%)	0/11 (0%)	0.15

AIH, artificial insemination by husband; ICSI, intracytoplasmic sperm injection; LOM, loss of methylation; OS, ovulation stimulation.

[a]Mann–Whitney *U*-test. Fisher's exact test was used for other analyses.

64).[11,12] In addition, we found that 30.0% of *H19*DMR-GOM patients showed MMDs, which is surprising considering that no MMDs were found in two previous reports in which 10 and 16 DMRs were analyzed.[8,11] These data suggest that the greater the number of DMRs analyzed, the higher the frequency of MMDs observed. In future, all DMRs in the genome should be analyzed to understand the precise frequency of MMDs, which DMRs become preferentially aberrantly methylated, and the mechanism by which MMDs occur.

In both *Kv*DMR1-LOM patients and *H19*DMR-GOM patients, we found MMDs in which not only LOM but also GOM were seen. We also found that both matDMRs and patDMRs were aberrantly methylated in both patient groups. It is noteworthy that matDMRs, probably gametic maternally methylated DMRs, were more susceptible to aberrant methylation than patDMRs in *Kv*DMR1-LOM patients, although no particular parent-based pattern of aberrant methylation has been reported previously.[12] This suggests that gametic maternally methylated DMRs are vulnerable to DNA demethylation during the preimplantation stage of early embryogenesis when *Kv*DMR1-LOM occurs.

Although it has not been reported that aberrant methylation of the corresponding DMR affects imprinted gene expression in MMD patients, we found biallelic expression of three imprinted genes (*ZDBF2*, *FAM50B*, and *GNAS1A*) to be associated with the aberrant methylation of their respective DMRs. Because biallelic expression increased the total expression levels of *ZDBF2* and *FAM50B*, we expect that had we measured the expression levels of *GNAS1A*, we would have observed an increase. Therefore, alteration of gene expression levels due to MMDs might affect the phenotype; however, clinical features between MMDs and monolocus methylation defects were not different in our study. This lack of difference has been previously reported,[7,9,10,13] although a few groups have reported a

difference in clinical features.[8,11,12] Two reasons for this similarity in terms of clinical features could be suggested. First, the mosaic ratio might be different in each organ. Because aberrant methylation was generally partial, it would occur after fertilization, and the patients would be mosaic. A high mosaic ratio would be a critical factor in the emergence of a distinct phenotype in BWS patients with monolocus methylation defects. Second, the imprinted locus at 11p15 might be epidominant over other imprinted loci because all MMD patients were clinically diagnosed as BWS.

Regarding the causative factor(s) for MMD, we could not find any pathological variation in any aberrantly methylated DMR, including *Kv*DMR1, suggesting that *cis*-acting variations of each specific DMR itself were not involved in the genesis of MMDs. On the other hand, the involvement of *trans*-acting factors has been advocated in other reports because mutations of *ZFP57* (which are required for the postfertilization maintenance of maternal and paternal methylation imprinting at multiple loci) have been found in transient neonatal diabetes mellitus type 1 patients with multilocus hypomethylation.[32] Mutations of *NLRP2* were also identified in a BWS patient with *Kv*DMR1-LOM and *MEST*-LOM in a family with complex consanguinity and in a Silver–Russell syndrome patient with multilocus hypomethylation.[12,33] In addition, TRIM28, NLRP7, KHDC3L, and DNMT3L have been considered to be candidate *trans*-acting factors. However, no mutations in any of these candidates or other genes, such as *DNMT1*, *DNMT3A*, and *DNMT3B*, were found in our BWS patients with MMDs, as determined by exome sequencing (K. Sasaki and K. Hata, personal communication). Recently, Lorthongpanich et al.[34] reported that the absence of maternal *Trim28* until zygotic gene activation at the two-cell late stage caused mosaicism of MMDs randomly, suggesting that insufficient expression of the candidate gene(s) at very early embryogenesis is an important event in the generation of MMDs in human imprinted diseases. Whole-genome sequencing and whole-genome bisulfite sequencing, including the regulatory regions of the candidate genes, and transcriptome analysis in early embryogenesis would be useful to identify the cause(s) of MMDs.

In our *H19*DMR-GOM patients, we also found GOM of *IGF2*-DMR0 and *IGF2*-DMR2 to be associated with GOM of *H19*DMR and *H19promoter* DMR, in agreement with previous reports.[22,35,36] Two patients showed simultaneous GOM at both *IGF2*-DMRs. Because *Igf2*-DMRs were established at the postimplantation stage under the control of *H19*DMR in mice,[37] GOM of *IGF2*-DMRs in BWS is likely to occur at the same stage. Although the function of *IGF2*-DMR0 is still unknown, methylated *Igf2*-DMR2 plays a role in transcription initiation of *Igf2* in mice.[38] GOM of the DMRs might change the high-order chromatin structure of the maternal allele and increase the expression of *IGF2* in cooperation with *H19*DMR-GOM in BWS patients.

In conclusion, our comprehensive and quantitative methylation analysis of multiple imprinted DMRs revealed several new findings: (i) matDMRs, probably gametic maternally methylated DMRs, are more susceptible to aberrant methylation during the preimplantation stage, when *Kv*DMR1-LOM occurs; (ii) aberrant methylation indeed alters imprinted gene expression; and (iii) *cis*-acting pathological variations of each DMR are not involved in the MMDs analyzed. Moreover, our study confirmed the simultaneous aberrant hypermethylation of *IGF2*-DMR0 and/or -DMR2 with isolated *H19*DMR-GOM. These findings may help us to understand the molecular mechanisms and pathophysiological features of MMDs.

SUPPLEMENTARY MATERIAL

Supplementary material is linked in the online version of the paper at http://www.nature.com/gim.

ACKNOWLEDGMENTS

We thank all the participants and their families who provided samples and all the doctors who referred patients to us. This study was supported, in part, by a Grant for Research on Intractable Diseases from the Ministry of Health, Labor, and Welfare; a Grant for Child Health and Development from the National Center for Child Health and Development; a Grant-in-Aid for Challenging Exploratory Research; and a Grant-in-Aid for Scientific Research (C) from the Japan Society for the Promotion of Science.

DISCLOSURE

The authors declare no conflict of interest.

REFERENCES

1. Abramowitz LK, Bartolomei MS. Genomic imprinting: recognition and marking of imprinted loci. *Curr Opin Genet Dev* 2012;22:72–78.
2. Tomizawa S, Sasaki H. Genomic imprinting and its relevance to congenital disease, infertility, molar pregnancy and induced pluripotent stem cell. *J Hum Genet* 2012;57:84–91.
3. Weksberg R, Shuman C, Beckwith JB. Beckwith-Wiedemann syndrome. *Eur J Hum Genet* 2010;18:8–14.
4. Choufani S, Shuman C, Weksberg R. Beckwith-Wiedemann syndrome. *Am J Med Genet C Semin Med Genet* 2010;154C:343–354.
5. Soejima H, Higashimoto K. Epigenetic and genetic alterations of the imprinting disorder Beckwith-Wiedemann syndrome and related disorders. *J Hum Genet* 2013;58:402–409.
6. Mackay DJ, Boonen SE, Clayton-Smith J, et al. A maternal hypomethylation syndrome presenting as transient neonatal diabetes mellitus. *Hum Genet* 2006;120:262–269.
7. Rossignol S, Steunou V, Chalas C, et al. The epigenetic imprinting defect of patients with Beckwith-Wiedemann syndrome born after assisted reproductive technology is not restricted to the 11p15 region. *J Med Genet* 2006;43:902–907.
8. Bliek J, Verde G, Callaway J, et al. Hypomethylation at multiple maternally methylated imprinted regions including PLAGL1 and GNAS loci in Beckwith-Wiedemann syndrome. *Eur J Hum Genet* 2009;17:611–619.
9. Azzi S, Rossignol S, Steunou V, et al. Multilocus methylation analysis in a large cohort of 11p15-related foetal growth disorders (Russell Silver and Beckwith Wiedemann syndromes) reveals simultaneous loss of methylation at paternal and maternal imprinted loci. *Hum Mol Genet* 2009;18:4724–4733.
10. Lim D, Bowdin SC, Tee L, et al. Clinical and molecular genetic features of Beckwith-Wiedemann syndrome associated with assisted reproductive technologies. *Hum Reprod* 2009;24:741–747.
11. Poole RL, Docherty LE, Al Sayegh A, et al.; International Clinical Imprinting Consortium. Targeted methylation testing of a patient cohort broadens the epigenetic and clinical description of imprinting disorders. *Am J Med Genet A* 2013;161:2174–2182.
12. Court F, Martin-Trujillo A, Romanelli V, et al. Genome-wide allelic methylation analysis reveals disease-specific susceptibility to multiple methylation defects in imprinting syndromes. *Hum Mutat* 2013;34:595–602.

13. Tee L, Lim DH, Dias RP, et al. Epimutation profiling in Beckwith-Wiedemann syndrome: relationship with assisted reproductive technology. *Clin Epigenetics* 2013;5:23.
14. DeBaun MR, Tucker MA. Risk of cancer during the first four years of life in children from The Beckwith-Wiedemann Syndrome Registry. *J Pediatr* 1998;132(3 Pt 1):398–400.
15. Soejima H, Nakagawachi T, Zhao W, et al. Silencing of imprinted CDKN1C gene expression is associated with loss of CpG and histone H3 lysine 9 methylation at DMR-LIT1 in esophageal cancer. *Oncogene* 2004;23:4380–4388.
16. Higashimoto K, Nakabayashi K, Yatsuki H, et al. Aberrant methylation of H19-DMR acquired after implantation was dissimilar in soma versus placenta of patients with Beckwith-Wiedemann syndrome. *Am J Med Genet A* 2012;158A:1670–1675.
17. Yatsuki H, Higashimoto K, Jozaki K, et al. Novel mutations of CDKN1C in Japanese patients with Beckwith-Wiedemann syndrome. *Genes & Genomics* 2013;35:141–147.
18. Higashimoto K, Jozaki K, Kosho T, et al. A novel de novo point mutation of the OCT-binding site in the IGF2/H19-imprinting control region in a Beckwith-Wiedemann syndrome patient. *Clin Genet* 2013; e-pub ahead of print 8 November 2013.
19. Ehrich M, Nelson MR, Stanssens P, et al. Quantitative high-throughput analysis of DNA methylation patterns by base-specific cleavage and mass spectrometry. *Proc Natl Acad Sci USA* 2005;102:15785–15790.
20. Rumbajan JM, Maeda T, Souzaki R, et al. Comprehensive analyses of imprinted differentially methylated regions reveal epigenetic and genetic characteristics in hepatoblastoma. *BMC Cancer* 2013;13:608.
21. Cui H, Onyango P, Brandenburg S, Wu Y, Hsieh CL, Feinberg AP. Loss of imprinting in colorectal cancer linked to hypomethylation of H19 and IGF2. *Cancer Res* 2002;62:6442–6446.
22. Murrell A, Ito Y, Verde G, et al. Distinct methylation changes at the IGF2-H19 locus in congenital growth disorders and cancer. *PLoS One* 2008;3: e1849.
23. Woodfine K, Huddleston JE, Murrell A. Quantitative analysis of DNA methylation at all human imprinted regions reveals preservation of epigenetic stability in adult somatic tissue. *Epigenetics Chromatin* 2011;4:1.
24. Reik W, Maher ER. Imprinting in clusters: lessons from Beckwith-Wiedemann syndrome. *Trends Genet* 1997;13:330–334.
25. Kobayashi H, Yamada K, Morita S, et al. Identification of the mouse paternally expressed imprinted gene Zdbf2 on chromosome 1 and its imprinted human homolog ZDBF2 on chromosome 2. *Genomics* 2009;93:461–472.
26. Nakabayashi K, Trujillo AM, Tayama C, et al. Methylation screening of reciprocal genome-wide UPDs identifies novel human-specific imprinted genes. *Hum Mol Genet* 2011;20:3188–3197.
27. Liu J, Litman D, Rosenberg MJ, Yu S, Biesecker LG, Weinstein LS. A GNAS1 imprinting defect in pseudohypoparathyroidism type IB. *J Clin Invest* 2000;106:1167–1174.
28. Demars J, Shmela ME, Rossignol S, et al. Analysis of the IGF2/H19 imprinting control region uncovers new genetic defects, including mutations of OCT-binding sequences, in patients with 11p15 fetal growth disorders. *Hum Mol Genet* 2010;19:803–814.
29. Weksberg R, Shuman C, Caluseriu O, et al. Discordant KCNQ1OT1 imprinting in sets of monozygotic twins discordant for Beckwith-Wiedemann syndrome. *Hum Mol Genet* 2002;11:1317–1325.
30. Tost J, Dunker J, Gut IG. Analysis and quantification of multiple methylation variable positions in CpG islands by Pyrosequencing. *Biotechniques* 2003;35:152–156.
31. Claus R, Wilop S, Hielscher T, et al. A systematic comparison of quantitative high-resolution DNA methylation analysis and methylation-specific PCR. *Epigenetics* 2012;7:772–780.
32. Mackay DJ, Callaway JL, Marks SM, et al. Hypomethylation of multiple imprinted loci in individuals with transient neonatal diabetes is associated with mutations in ZFP57. *Nat Genet* 2008;40:949–951.
33. Meyer E, Lim D, Pasha S, et al. Germline mutation in NLRP2 (NALP2) in a familial imprinting disorder (Beckwith-Wiedemann Syndrome). *PLoS Genet* 2009;5:e1000423.
34. Lorthongpanich C, Cheow LF, Balu S, et al. Single-cell DNA-methylation analysis reveals epigenetic chimerism in preimplantation embryos. *Science* 2013;341:1110–1112.
35. Reik W, Brown KW, Schneid H, Le Bouc Y, Bickmore W, Maher ER. Imprinting mutations in the Beckwith-Wiedemann syndrome suggested by altered imprinting pattern in the IGF2-H19 domain. *Hum Mol Genet* 1995;4:2379–2385.
36. Sparago A, Russo S, Cerrato F, et al. Mechanisms causing imprinting defects in familial Beckwith-Wiedemann syndrome with Wilms' tumour. *Hum Mol Genet* 2007;16:254–264.
37. Lopes S, Lewis A, Hajkova P, et al. Epigenetic modifications in an imprinting cluster are controlled by a hierarchy of DMRs suggesting long-range chromatin interactions. *Hum Mol Genet* 2003;12:295–305.
38. Murrell A, Heeson S, Bowden L, et al. An intragenic methylated region in the imprinted Igf2 gene augments transcription. *EMBO Rep* 2001;2:1101–1106.

CLINICAL GENETICS An International Journal of Genetics, Molecular and Personalized Medicine

Clin Genet 2014: 86: 539–544
Printed in Singapore. All rights reserved

CLINICAL GENETICS
doi: 10.1111/cge.12318

Short Report

A novel *de novo* point mutation of the OCT-binding site in the *IGF2/H19*-imprinting control region in a Beckwith–Wiedemann syndrome patient

Higashimoto K., Jozaki K., Kosho T., Matsubara K., Fuke T., Yamada D., Yatsuki H., Maeda T., Ohtsuka Y., Nishioka K., Joh K., Koseki H., Ogata T., Soejima H. A novel *de novo* point mutation of the OCT-binding site in the *IGF2/H19*-imprinting control region in a Beckwith–Wiedemann syndrome patient.
Clin Genet 2014: 86: 539–544. © John Wiley & Sons A/S. Published by John Wiley & Sons Ltd, 2013

The *IGF2/H19*-imprinting control region (ICR1) functions as an insulator to methylation-sensitive binding of CTCF protein, and regulates imprinted expression of *IGF2* and *H19* in a parental origin-specific manner. ICR1 methylation defects cause abnormal expression of imprinted genes, leading to Beckwith–Wiedemann syndrome (BWS) or Silver–Russell syndrome (SRS). Not only ICR1 microdeletions involving the CTCF-binding site, but also point mutations and a small deletion of the OCT-binding site have been shown to trigger methylation defects in BWS. Here, mutational analysis of ICR1 in 11 BWS and 12 SRS patients with ICR1 methylation defects revealed a novel *de novo* point mutation of the OCT-binding site on the maternal allele in one BWS patient. In BWS, all reported mutations and the small deletion of the OCT-binding site, including our case, have occurred within repeat A2. These findings indicate that the OCT-binding site is important for maintaining an unmethylated status of maternal ICR1 in early embryogenesis.

Conflict of interest

The authors have no competing financial interests to declare.

K. Higashimoto[a], K. Jozaki[a], T. Kosho[b], K. Matsubara[c], T. Fuke[c], D. Yamada[d], H. Yatsuki[a], T. Maeda[a], Y. Ohtsuka[a], K. Nishioka[a], K. Joh[a], H. Koseki[d], T. Ogata[e] and H. Soejima[a]

[a]Division of Molecular Genetics & Epigenetics, Department of Biomolecular Sciences, Faculty of Medicine, Saga University, Saga, Japan, [b]Department of Medical Genetics, Shinshu University School of Medicine, Matsumoto, Nagano, Japan, [c]Department of Molecular Endocrinology, National Research Institute for Child Health and Development, Tokyo, Japan, [d]Laboratory for Developmental Genetics, RIKEN Center for Integrative Medical Sciences (IMS), Yokohama, Kanagawa, Japan, and [e]Department of Pediatrics, Hamamatsu University School of Medicine, Hamamatsu, Japan

Key words: Beckwith–Wiedemann syndrome – ICR1 methylation defect – *IGF2/H19* – OCT-binding site – Silver–Russell syndrome

Corresponding author: Hidenobu Soejima, Division of Molecular Genetics & Epigenetics, Department of Biomolecular Sciences, Faculty of Medicine, Saga University, 5-1-1 Nabeshima, Saga 849–8501, Japan.
Tel.: +81 952 34 2260;
fax: +81 952 34 2067;
e-mail: soejimah@cc.saga-u.ac.jp

Received 5 August 2013, revised and accepted for publication 6 November 2013

Human 11p15 contains two neighboring imprinted domains, *IGF2/H19* and *KCNQ1*. Each domain is controlled by its own imprinting control region: ICR1 or ICR2, respectively (1). ICR1 methylation defects cause abnormal imprinted expression of insulin-like growth factor 2 (*IGF2*), which encodes a growth factor, and non-coding RNA *H19*, which possesses possible tumor-suppressor functions, leading to Beckwith–Wiedemann syndrome (BWS: OMIM 130650) and Silver–Russell syndrome (SRS: OMIM 180860), respectively (1, 2).

BWS is a congenital overgrowth disorder characterized by macroglossia, macrosomia, and abdominal wall defects, whereas SRS is a congenital growth retardation disorder characterized by a typical facial gestalt, clinodactyly V, and body asymmetry (1, 2). Among varied causative genetic and epigenetic abnormalities, ICR1 methylation defects are etiologies common to both diseases. Gain of methylation (GOM) and loss of methylation (LOM) at ICR1 account for ~5% of BWS and ~44% of SRS cases, respectively (1, 2).

ICR1 upstream of *H19* is a differentially methylated region (DMR) that is methylated exclusively on the paternal allele, and it regulates the imprinted expression of paternally expressed *IGF2* and maternally expressed *H19*. On the maternal allele, unmethylated ICR1 bound by CTCF forms a chromatin insulator that prevents *IGF2* promoter activation by the enhancer downstream of *H19*, resulting in silencing of *IGF2* and activation of *H19*. On the paternal allele, methylation-sensitive CTCF cannot bind to methylated ICR1, resulting in activation of *IGF2* and silencing of *H19* (3, 4). CTCF also maintains the unmethylated status of ICR1 on the maternal allele (5, 6).

Human ICR1 contains two different repetitive sequences (A and B) and seven CTCF-binding sites (CTSs) (Fig. 1a). A maternally inherited ICR1 microdeletion (1.4–2.2 kb), which affects ICR1 function and CTCF binding by changing CTS spacing, has been reported to result in ICR1-GOM in a few familial BWS cases (7–9). ICR1 also contains other protein-binding motifs, such as OCT, SOX, and ZFP57 (10, 11). Recently, point mutations and a small deletion of the OCT or SOX motif have been reported in a few BWS patients with ICR1-GOM (10, 12, 13).

Here, mutational analysis in 11 BWS and 12 SRS patients with ICR1 methylation defects revealed a novel *de novo* point mutation in the OCT-binding site on the maternal allele of one BWS patient.

Materials and methods

Patients

Eleven BWS and twelve SRS patients, who were clinically diagnosed, were enrolled in this study. All BWS and SRS patients displayed isolated GOM and LOM of ICR1, respectively. This study was approved by the Ethics Committee for Human Genome and Gene Analyses of the Faculty of Medicine, Saga University. Written informed consents were obtained from the parents or guardians of the patients.

Sequencing analysis of ICR1

A genomic region in and around ICR1, which included seven CTSs and three OCT-binding sites, was directly sequenced in all patients as previously described (14). All polymerase chain reaction (PCR) primer pairs used are listed in Table S1, Supporting Information.

Microsatellite analysis

For quantitative polymorphism analysis, tetranucleotide repeat markers, *D11S1984* at 11p15.5 and *D11S1997* at 11p15.4, were amplified and analyzed with GeneMapper software. The peak height ratios of the paternal allele to the maternal allele were calculated.

Southern blot analysis

Methylation-sensitive Southern blots with *Pst*I/*Mlu*I and *Bam*HI/*Not*I were employed for ICR1 and ICR2, respectively, as described previously (15). Band intensity was measured using a FLA-7000 fluoro-image analyzer (Fujifilm, Tokyo, Japan). The methylation index (MI, %) was then calculated.

Bisulfite sequencing

Bisulfite sequencing was performed covering the three variants within ICR1 that were found in BWS-s043. Genomic DNA was bisulfite-converted using an EpiTect Bisulfite Kit (Qiagen, Hilden, Germany). After PCR amplification, the products were cloned and sequenced.

Electrophoretic mobility shift assay

The pCMX-Flag-human OCT4 and pCMX-Flag-human SOX2 were simultaneously transfected into HEK293 cells. The nuclear extracts from HEK293 cells expressing human OCT4/SOX2 and mouse ES cells were used. Electrophoretic mobility shift assay (EMSA) was performed as described previously (10). For supershift analysis, 1.5 µg of anti-OCT4 antibody (Abcam, ab19857, Cambridge, UK) or 1.5 µg of anti-SOX2 antibody (R&D systems, AF2018, Minneapolis, MN) was used. The unlabeled probes were also used as competitors. The reaction mixtures were separated on a 4% polyacrylamide gel and exposed to a film. Oligonucleotide sequences are presented in Table S1.

Results

Among 11 BWS and 12 SRS patients with ICR1 methylation defects, 7 and 2 variants from 5 BWS and 2 SRS patients were found, respectively (Table 1). The variants in BWS-047 and BWS-s061 were polymorphisms. The remaining variants were not found in the normal population, the UCSC Genome Browser database, or the 1000 Genomes database, suggesting them to be candidates for causative mutations for ICR1 methylation defects. However, the positions of the variants, except

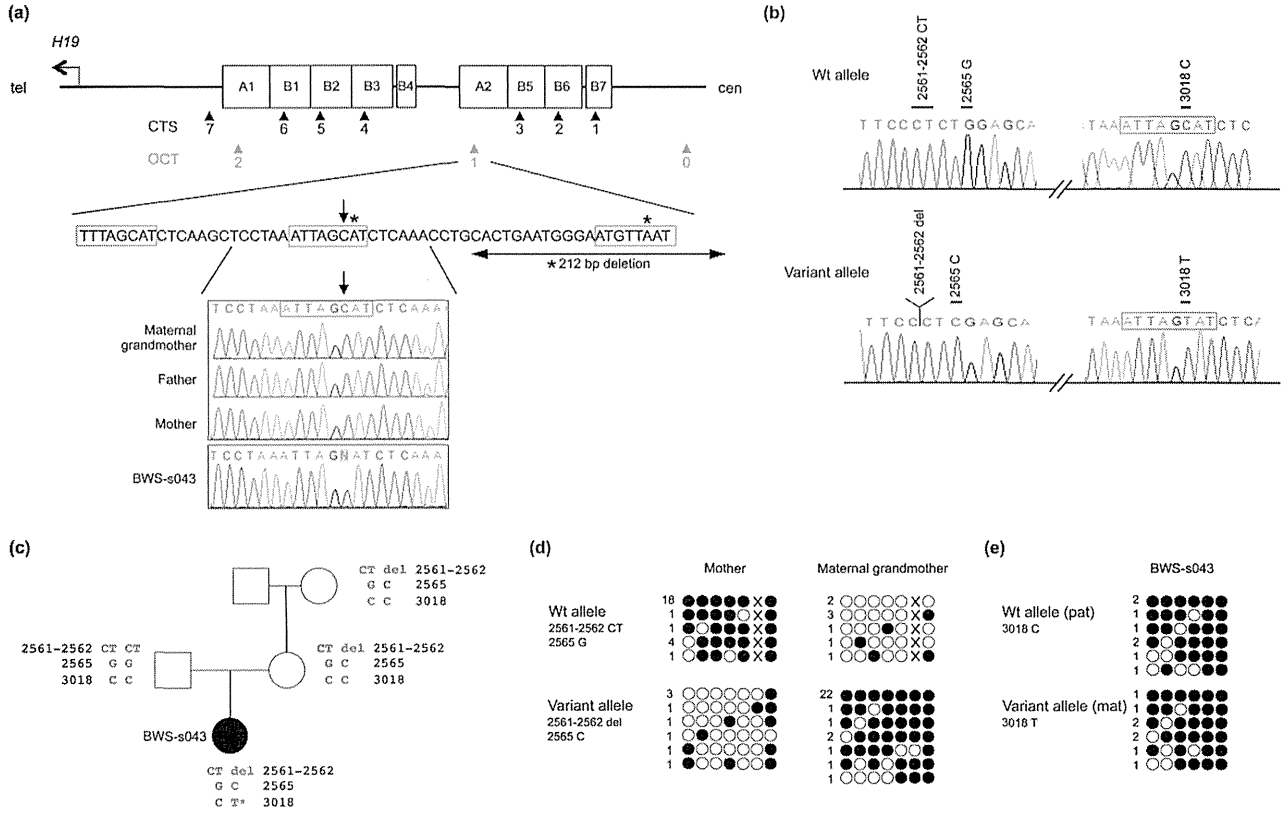

Fig. 1. The three variants in BWS-s043 and their effects on ICR1 methylation. (**a**) Map of ICR1 and the position of 2,023,018C>T. Upper panel: structure of ICR1. ICR1 consists of two repeat blocks. Each block consists of one repeat A and three or four repeat Bs. The black and red arrowheads indicate CTCF-binding sites (CTS) and OCT-binding sites (OCT), respectively. Middle panel: the position of 2,023,018C>T (arrow) and previously reported mutations and deletions (asterisks). Three octamer motifs are enclosed by a red line. Lower panel: electrophoretograms around 2,023,018C>T. BWS-s043 were heterozygous for the variant, whereas the maternal grandmother and both parents did not harbor it. (**b**) Haplotype encompassing the three variants in BWS-s043. Polymerase chain reaction (PCR) products encompassing the three variants were cloned and sequenced. All three variants were revealed to be on the same allele in BWS-s043. (**c**) Pedigree and haplotype of the family. Haplotype analysis showed that 2,023,018C>T (asterisk) occurred on the maternal allele in BWS-s043. (**d**) Bisulfite sequencing analysis encompassing the 2,022,561-562CT>delCT and the 2,022,565G>C variants in the mother and the maternal grandmother. Open and filled circles indicate unmethylated and methylated CpG sites, respectively. X indicates G at chr11: 2,022,565. Numerals on the left reflect the number of clones with the same methylation pattern. The variant allele was unmethylated in the mother and methylated in the maternal grandmother, respectively. (**e**) Bisulfite sequencing analysis encompassing 2,023,018C>T in BWS-s043. The maternal allele contained a *de novo* variant that was heavily methylated in BWS-s043, while differential methylation was maintained in other family members and normal controls without the variant (Fig. S2a).

Table 1. Variants found in this study[a]

Patient ID	MI of ICR1 (%)	Variant	Position (GRCh37/hg19 chr11)	Location	Transmission	Heterozygosity in normal population
BWS-047	100	G>Gdel	2,024,428	Centromeric outside of ICR1 (5′ of CTS1)	Maternal	2/116 (rs200288360)
		CT>CT del	2,022,561–2,022,562	Between A2 and B4	Maternal	na
BWS-s043	86	G>C	2,022,565	Between A2 and B4	Maternal	0/115
		C>T	2,023,018	A2 (OCT-binding site 1)	*De novo*	0/107
BWS-s061	76	C>T	2,023,497	B5 (5′ of CTS3)	Paternal	2/105
BWS-s081	67	C>T	2,025,777	Centromeric outside of ICR1 (3′ of OCT-binding site 0)	Paternal	0/106
BWS-s100	67	C>A	2,021,145	B1 (3′ of CTS6)	Maternal	0/105
SRS-002	4	G>Gdel	2,024,364	B7 (5′ of CTS1)	Unknown	0/106
SRS-s03	24	C>T	2,021,103	B1 (3′ of CTS6)	Maternal	0/106

ICR, imprinting control region; MI, methylation index; na, not analyzed.
[a]Parents' DNA were not available for SRS-002.

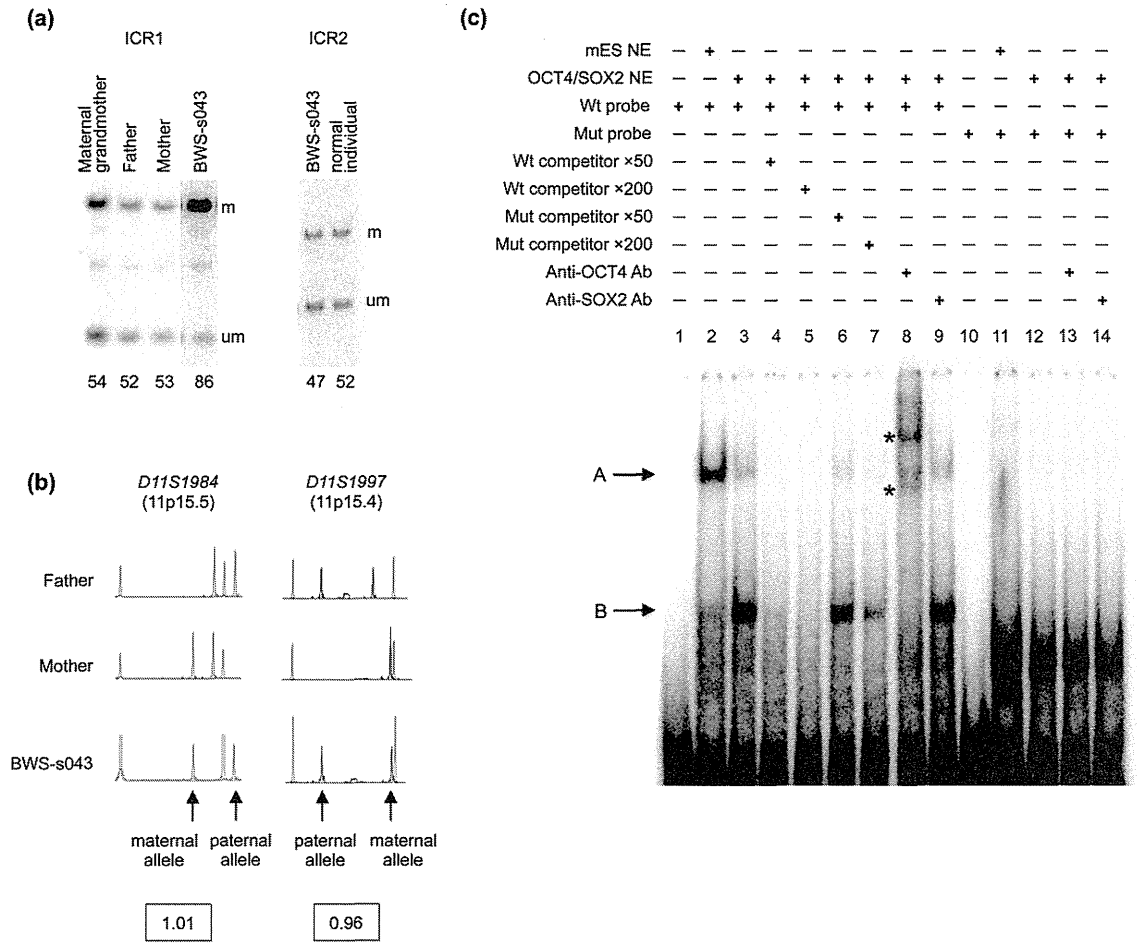

Fig. 2. Methylation-sensitive Southern blots and microsatellite analysis of BWS-s043, and electrophoretic mobility shift assay (EMSA) for 2,023,018C>T. (**a**) Methylation-sensitive Sothern blots of ICR1 and ICR2. Methylation indices [MI, %] are shown below each lane. MI was calculated using the equation $M/(M+U) \times 100$, where M is the intensity of the methylated band and U is the intensity of the unmethylated band. m, methylated band; um, unmethylated band. BWS-s043 showed ICR1-GOM, whereas the relatives did not. Methylation statuses of CTS1 and CTS4 are shown in Fig. S2b,c. Methylation of ICR2 in BWS-s043 was normal. (**b**) Microsatellite analysis at 11p15.4-p15.5. Ratios of the paternal allele to the maternal allele in BWS-s043 were approximately 1, indicating no uniparental disomy. Red peaks are molecular markers. (**c**) EMSA using the wild-type (Wt) probe and the mutant (Mut) probe encompassing 2,023,018C>T. The unlabeled Wt probe or Mut probe (×50 or ×200 molar excess) was used as a competitor. The arrows and asterisks indicate the protein-DNA complexes (A and B) and supershifted complexes, respectively. mES NE, nuclear extract from mouse ES cells; OCT4/SOX2 NE, nuclear extract from human HEK293 cells expressing OCT4/SOX2; Ab, antibody.

for BWS-s043, were not located at any protein-binding sites that have been reported as involved in methylation imprinting (CTCF, OCT, and ZFP57) (3, 4, 10, 12, 16). Furthermore, we did not find any protein-oligonucleotide complexes in EMSA using mouse ES nuclear extracts and oligonucleotide probes encompassing all variants, except for BWS-s043 (Fig. S1). Therefore, we analyzed further three variants in BWS-s043, which were in and around the OCT-binding site 1.

First, we re-confirmed that BWS-s043 showed GOM near CTS6 within ICR1, but it did not demonstrate LOM at ICR2, paternal uniparental disomy of chromosome 11, or a *CDKN1C* mutation (Fig. 2a,b, and data not shown). The 2,023,018C>T variant was located in the second octamer motif of OCT-binding site 1 within repeat A2 (Fig. 1a). The other two variants were located approximately 450 bp on the telomeric side of the 2,023,018C>T variant, between repeats A2 and B4 (Fig. 1a, Table 1). The 2,023,018C>T variant was absent in other family members, indicating a *de novo* variant (Fig. 1a). To clarify if the *de novo* variant in the patient occurred on the maternal or paternal allele, we performed haplotype analysis with PCR covering all three variants. We found all three variants were located on the same allele and the 2,023,018C>T variant occurred *de novo* on the maternal allele because the 2,022,561–562CT>delCT and 2,022,565G>C variants were on the maternal allele in the patient (Fig. 1b,c).

Next, we investigated the methylation status of ICR1. Methylation-sensitive Southern blots and bisulfite sequencing showed normal methylation of ICR1 in the parents and the maternal grandmother (Figs 2a and S2). As for the 2,022,561-562CT>delCT and the 2,022,565G>C variants, the variant allele was unmethylated in the mother, but methylated in the grandmother (Fig. 1d). On the basis of methylation

analysis, the variant allele in the grandmother must have been transmitted by her father, and that in the mother must have been transmitted by her mother. The results indicated that the variant allele could be either methylated or unmethylated during gametogenesis, strongly suggesting no relation between the variants and ICR1-GOM. On the other hand, bisulfite sequencing including the 2,023,018C>T variant revealed that both the variant and wild-type alleles were heavily methylated in the patient (Fig. 1e), while differential methylation was maintained in other family members and normal controls without the variant (Fig. S2a). As the *de novo* variant on the maternal allele was located within the OCT-binding site, which is required for the maintenance of the unmethylated status in a mouse model, the variant was likely involved in ICR1-GOM (17, 18).

Finally, we performed EMSA to determine if 2,023,018C>T influenced the binding ability of nuclear protein factors, such as OCT4 and SOX2 (Fig. 2c). The wild-type probe formed two complexes (A and B) with the nuclear extracts of mouse ES cells and HEK293 cells expressing OCT4/SOX2 (lanes 2 and 3), whereas such complexes were not observed in the mutant probe (lanes 11 and 12). Complexes A and B competed more efficiently with wild-type than with the mutant competitor (lanes 4 to 7). Furthermore, complex B, but not A, was supershifted with the antibody against OCT4 (lane 8). The supershift did not occur with the antibody against SOX2 and with both antibodies using the mutant probe (lanes 9, 13, and 14). These data demonstrated that 2,023,018C>T abrogated binding ability of a nuclear factor, most likely OCT4. Taken together, our data strongly suggest that 2,023,018C>T is a mutation that could prevent OCT4 binding to the OCT-binding site and induce ICR1-GOM, leading to BWS.

Discussion

We identified a novel *de novo* point mutation, chr11: 2,023,018C>T, in OCT-binding site 1 within repeat A2 in a BWS patient with ICR1-GOM. Our data strongly suggest the involvement of the mutation in GOM at ICR1. In a mouse cell model, the evolutionarily well-conserved dyad octamer motif within ICR1, which is bound by OCT protein, has been shown to be required for the maintenance of unmethylated status competing against *de novo* methylation (17). In addition, the importance of a SOX motif flanked by an OCT motif has also been reported (19). Recent studies have shown that the SOX–OCT motif functions to maintain unmethylated status *in vitro* and *in vivo*; a cooperative function of CTCF and OCT/SOX for maintenance of differential methylation has been suggested as responsible (18, 19). Although there is one OCT-binding site in mice, three evolutionarily conserved OCT-binding sites (0, 1, 2) are located in and around ICR1 in humans. As all mutations and the small deletion previously reported in addition to our case occurred in site 1 within repeat A2 (Fig. 1a), site 1 within repeat A2 likely plays a more important role for maintaining unmethylated status of maternal ICR1 in humans than the other OCT-binding sites (10, 12, 13).

ICR1-GOM cases, including ours, with mutations/deletions also show partial hypermethylation in spite of pre-existent genetic aberrations in the oocyte (9, 12, 13, 20), suggesting aberrant hypermethylation at ICR1 would also be stochastically acquired at a cellular level even in the existence of such aberrations.

As for SRS, including familial cases, the ICR1 mutation has not been found except in one sporadic case to date (10). We did not find any promising mutations in this study, suggesting the cause of ICR1 methylation defects to differ between SRS and BWS.

In conclusion, we identified a novel *de novo* point mutation of OCT-binding site 1 within repeat A2, a location suggested to play an important role for maintaining the unmethylated status of maternal ICR1 in humans, on the maternal allele in a BWS patient with ICR1-GOM. However, genetic aberrations of ICR1 explain only 20% of BWS cases with ICR1-GOM (10). As aberrant methylation may occur as a consequence of stochastic events or environmental influences irrespective of ICR1 mutations, unknown causes for ICR1 methylation defects should be clarified.

Supporting Information

The following Supporting information is available for this article:

Fig. S1. EMSA for all variants found in this study, except for those in BWS-047 and BWS-s061, using the nuclear extract from mouse ES cells. The variant in BWS-s081 was located outside of ICR1, and a CpG site within the probe sequence was mostly unmethylated in three normal controls (data not shown). Thus, an unmethylated probe was used for it. Since the variants in BWS-s100 and SRS-s03 were located 3′ of CTS6 and found on the maternal allele, unmethylated probes were used for them. As for the variant in SRS-002, it was located 5′ of CTS1 but its parental origin was unknown. Thus, both unmethylated and methylated probes were used for it. There was no difference between a wt-probe and a variant-probe in each variant except for the BWS-s043 mutation. A wt-probe for the BWS-s043 mutation formed two complexes, whereas such complexes were not observed with a probe for the mutation. These results suggested that only the BWS-s043 mutation affected the protein–DNA interaction (see text and Fig. 2c for details). WT, probe for the wild-type sequence; MUT, probe for the BWS-s043 mutation; VAR, probe for the variant sequence; um, unmethylated probe; me, methylated probe; mES NE, nuclear extract from mouse ES cells.
Fig. S2. Bisulfite sequencing of the region encompassing the 2,023,018 variant, CTS1, and CTS4. (**a**) Results for the 2,023,018 variant. In the healthy members of the BWS-s043 family, comprised of the maternal grandmother, mother, and father, showed differential methylation. Three normal controls also showed differential methylation. In particular, normal control 3 was heterozygous for a SNP (rs61520309) and showed differential methylation in an allele-dependent manner. Open and filled circles indicate unmethylated and methylated CpG sites, respectively. (**b**) Results for CTS1. Two normal controls that were heterozygous for a SNP (rs2525885) showed differential methylation. The healthy family members also showed differential methylation, whereas the patient, BWS-s043, showed aberrant hypermethylation. CpG sites within CTS1 are indicated by a short horizontal line. X indicates T of the SNP (rs2525885). (**c**) Results for CTS4. The healthy family members and two normal controls showed differential

methylation. Among them, the parents and two normal controls were heterozygous for a SNP (rs2525883). The patient, BWS-s043, showed aberrant hypermethylation. CpG sites within CTS4 were indicated by a short horizontal line. X indicates T of the SNP (rs2525883).
Table S1. PCR primers and oligonucleotide probes used in this study.

Additional Supporting information may be found in the online version of this article.

Acknowledgements

This study was supported, in part, by a Grant for Research on Intractable Diseases from the Ministry of Health, Labor, and Welfare; a Grant for Child Health and Development from the National Center for Child Health and Development; a Grant-in-Aid for Challenging Exploratory Research; and, a Grant-in-Aid for Scientific Research (C) from the Japan Society for the Promotion of Science.

References

1. Weksberg R, Shuman C, Beckwith JB. Beckwith–Wiedemann syndrome. Eur J Hum Genet 2010: 18: 8–14.
2. Gicquel C, Rossignol S, Cabrol S et al. Epimutation of the telomeric imprinting center region on chromosome 11p15 in Silver–Russell syndrome. Nat Genet 2005: 37: 1003–1007.
3. Bell AC, Felsenfeld G. Methylation of a CTCF-dependent boundary controls imprinted expression of the Igf2 gene. Nature 2000: 405: 482–485.
4. Hark AT, Schoenherr CJ, Katz DJ, Ingram RS, Levorse JM, Tilghman SM. CTCF mediates methylation-sensitive enhancer-blocking activity at the H19/Igf2 locus. Nature 2000: 405: 486–489.
5. Schoenherr CJ, Levorse JM, Tilghman SM. CTCF maintains differential methylation at the Igf2/H19 locus. Nat Genet 2003: 33: 66–69.
6. Pant V, Mariano P, Kanduri C et al. The nucleotides responsible for the direct physical contact between the chromatin insulator protein CTCF and the H19 imprinting control region manifest parent of origin-specific long-distance insulation and methylation-free domains. Genes Dev 2003: 17: 586–590.
7. Sparago A, Cerrato F, Vernucci M, Ferrero GB, Silengo MC, Riccio A. Microdeletions in the human H19 DMR result in loss of IGF2 imprinting and Beckwith–Wiedemann syndrome. Nat Genet 2004: 36: 958–960.
8. Prawitt D, Enklaar T, Gärtner-Rupprecht B et al. Microdeletion of target sites for insulator protein CTCF in a chromosome 11p15 imprinting center in Beckwith–Wiedemann syndrome and Wilms' tumor. Proc Natl Acad Sci U S A 2005: 102: 4085–4090.
9. Beygo J, Citro V, Sparago A et al. The molecular function and clinical phenotype of partial deletions of the IGF2/H19 imprinting control region depends on the spatial arrangement of the remaining CTCF-binding sites. Hum Mol Genet 2013: 22: 544–557.
10. Demars J, Shmela ME, Rossignol S et al. Analysis of the IGF2/H19 imprinting control region uncovers new genetic defects, including mutations of OCT-binding sequences, in patients with 11p15 fetal growth disorders. Hum Mol Genet 2010: 19: 803–814.
11. Quenneville S, Verde G, Corsinotti A et al. In embryonic stem cells, ZFP57/KAP1 recognize a methylated hexanucleotide to affect chromatin and DNA methylation of imprinting control regions. Mol Cell 2011: 44: 361–372.
12. Poole RL, Docherty LE, Al Sayegh A et al. Targeted methylation testing of a patient cohort broadens the epigenetic and clinical description of imprinting disorders. Am J Med Genet A 2013: 161: 2174–2182.
13. Berland S, Appelbäck M, Bruland O et al. Evidence for anticipation in Beckwith–Wiedemann syndrome. Eur J Hum Genet 2013: 21: 1344–1348.
14. Higashimoto K, Nakabayashi K, Yatsuki H et al. Aberrant methylation of H19-DMR acquired after implantation was dissimilar in soma versus placenta of patients with Beckwith–Wiedemann syndrome. Am J Med Genet A 2012: 158A: 1670–1675.
15. Soejima H, Nakagawachi T, Zhao W et al. Silencing of imprinted CDKN1C gene expression is associated with loss of CpG and histone H3 lysine 9 methylation at DMR-LIT1 in esophageal cancer. Oncogene 2004: 23: 4380–4388.
16. Mackay DJ, Callaway JL, Marks SM et al. Hypomethylation of multiple imprinted loci in individuals with transient neonatal diabetes is associated with mutations in ZFP57. Nat Genet 2008: 40: 949–951.
17. Hori N, Nakano H, Takeuchi T et al. A dyad Oct-binding sequence functions as a maintenance sequence for the unmethylated state within the H19/Igf2-imprinted control region. J Biol Chem 2002: 277: 27960–27967.
18. Sakaguchi R, Okamura E, Matsuzaki H, Fukamizu A, Tanimoto K. Sox-Oct motifs contribute to maintenance of the unmethylated H19 ICR in YAC transgenic mice. Hum Mol Genet 2013: 22: 4627–4637.
19. Hori N, Yamane M, Kouno K, Sato K. Induction of DNA demethylation depending on two sets of Sox2 and adjacent Oct3/4 binding sites (Sox-Oct motifs) within the mouse H19/insulin-like growth factor 2 (Igf2) imprinted control region. J Biol Chem 2012: 287: 44006–44016.
20. Sparago A, Russo S, Cerrato F et al. Mechanisms causing imprinting defects in familial Beckwith–Wiedemann syndrome with Wilms' tumour. Hum Mol Genet 2007: 16: 254–264.